ATTRIBUTION & QUANTIFICATION OF CH_4 EMISSIONS IN THE PORT OF AMSTERDAM

MSc Thesis
06-07-2022

Project by Daan Stroeken
Supervised by Hossein Maazallahi, Thomas Röckmann & Guus Velders

TNO innovation for life
Utrecht University
Sharing science, shaping tomorrow

Abstract

Reducing methane (CH_4) emissions is a major part of the short-term international agreements in mitigating climate change. Minimising industry emissions could be a logical strategy, but inventorying and verifying methane emissions on the scale of individual facilities is challenging in industry-dense/urban areas. Mobile measurements can provide a fast solution in the detection, attribution and quantification of methane emissions of individual facilities. In a non-continuous 14-day campaign, we measured CH_4, ethane (C_2H_6) and carbon dioxide (CO_2) mole fractions around 19 facilities in the Port of Amsterdam, using Picarro G2301 and Picarro G4302 Cavity Ring-Down Spectroscopy (CRDS) analysers in a mobile van. Crosswind transects were conducted downwind of a facility if the road structure allowed, and using a Gaussian Plume Dispersion Model (GPDM,) 9 emission points were quantified. Meteorological data from the KNMI WRF model and a KNMI Schiphol tower were to compare the two datasets' quantified emission rates. The combination of 2 CRDS analysers and 2 meteorological datasets led to 4 average emission rates per facility.

We identified methane emissions at 15 facilities in the area, of which 7 were not registered in the national inventory. Three wastewater treatment plants (WWTPs) with registered emissions were quantified. The largest WWTP was quantified at about half the registered rate, with a maximum rate of 25.6 ± 2.6 kg CH_4 h^{-1}. The other two WWTPs were similar to or just above their registered rate. The other 6 facilities, for which the emissions could be attributed with certainty, were not registered. At least three facilities were estimated to emit more than WWTP, the largest registered emitter. Landfill Nauerna emissions, which have been measured in earlier campaigns, were estimated between 88.3 ± 10.6 and 105.7 ± 14.0 kg CH_4 h^{-1}. Two coal transhipment terminals, a cacao processer, a biogas producer and an organic waste collector all emitted more than WWTP Zaandam, the lowest registered facility. The estimated emissions for those locations ranged between 9.6 – 83.4 kg CH_4 h^{-1}. The results show that mobile measurements can be used to cross-check emission reports and identify unreported locations.

1 Inhoud

2 Introduction

2.1 Global increase in atmospheric CO_2 and CH_4

Human activities lead to the emission of greenhouse gasses such as carbon dioxide (CO_2) and methane (CH4). Since pre-industrial times, atmospheric CH_4 mole fractions have increased from 722 ppb in 1750 - 1800 to 1900 ppb in September 2021 (Dlugokencky, 2021; Myhre et al., 2013). This causes increases in radiative forcing and leads to a warming climate (Stocker et al., 2013; Turner et al., 2019).

About 50% to 65% of all methane emissions are estimated to come from anthropogenic sources (Stocker et al., 2013). The global methane mixing ratio is low compared to carbon dioxide (about 400 ppm), but the global warming potential (GWP) of methane is 84 larger than that of carbon dioxide on a 20-year time scale (Dlugokencky, 2021; Turner et al., 2019). This makes methane the second most important anthropogenic greenhouse gas, contributing 23% of the additional radiative forcing since preindustrial times (Etminan et al., 2016; Myhre et al., 2013; Ocko et al., 2021).

Methane mitigation measures are attractive because the short atmospheric lifetime of methane means that such measures would have a fast impact on reducing global warming. The recent COP26 in Glasgow affirms the importance of methane reduction measures, which stated the ambition of reducing methane emissions by 30% in 2030 (UNFCC, 2021). This could avoid global warming by 0.25 °C in 2050 and by 0.5 °C by the end of the century (Ocko et al., 2018). Reducing methane emissions could play a significant role in reaching the ambitious goal of the Paris Agreement, to keep the rise of global temperature below 2 °C (UNFCC, 2015).

In the past 50 years, the atmospheric methane mixing ratio increased until the late ’90s but stabilised in the 00s. Around 2007 the concentration started growing again, with larger growth rates each year (Nisbet et al., 2019). In 2020, the methane mixing ratio grew by 15 ppb/year, the most significant growth in 40 years and 50% larger than in 2019 (Figure 1) (Dlugokencky, 2021).

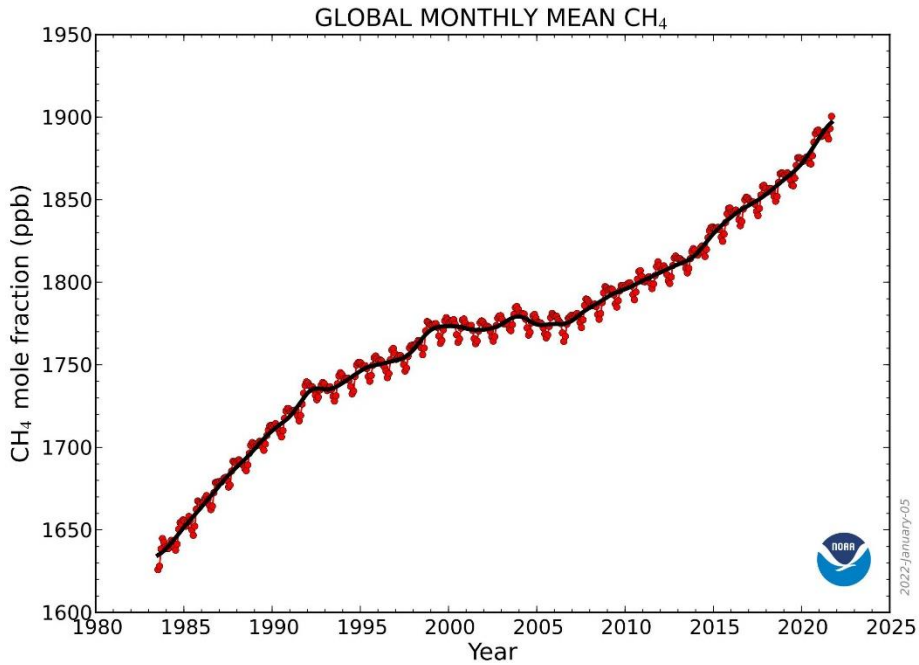

Figure 1. The increase of the atmospheric dry air mole fraction since 1980. The figure shows stabilisation until around 2007, after which the growth started increasing again, with 2021 showing the highest growth rate since 1990 (Dlugokencky, 2021).

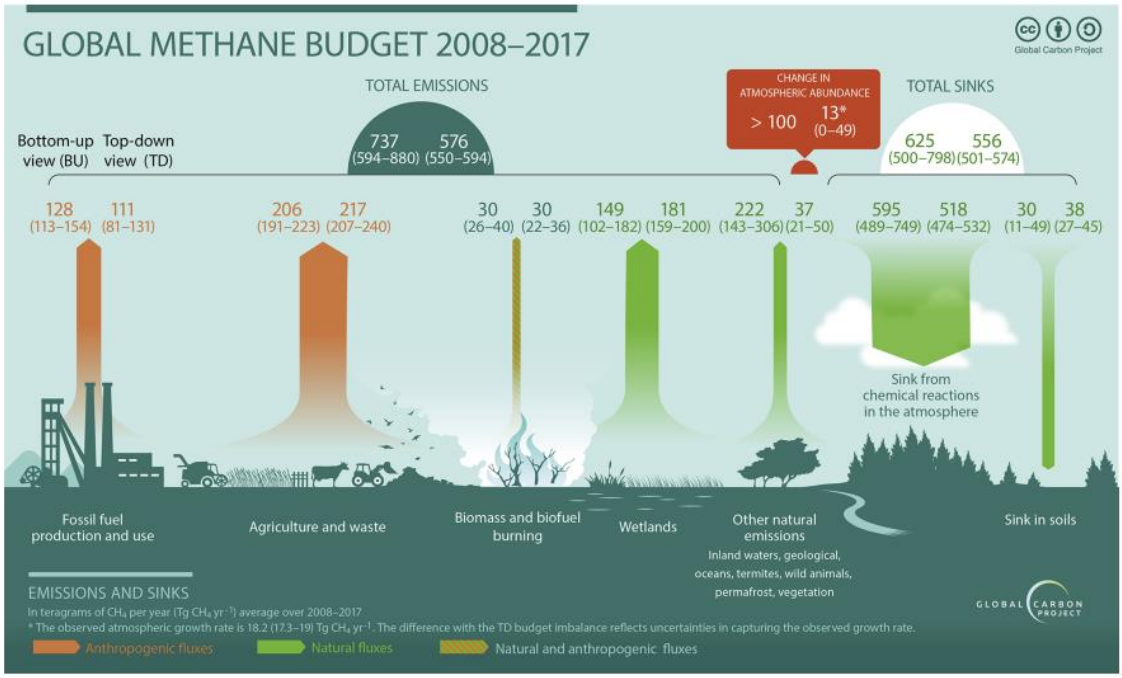

Figure 2. An overview of the different sources and sinks of atmospheric methane (Tg CH_4 yr^{-1}) and the differences between top-down and bottom-up methods. From the Global Methane Budget, figure 6 (Saunois et al., 2020).

2.2 Sources of methane emissions

The Global Methane Budget reports on changes in all atmospheric methane sources and sinks globally (Saunois et al., 2020). Figure 2 shows the most important anthropogenic source categories: fugitive emissions during fossil fuel production and use, agriculture, waste and biomass/-fuel burning. Wetlands are the largest source of natural emissions. Bottom-up methods estimate the total global methane emissions to be 737 Tg CH_4 yr^{-1} in 2008-2017, which is about 160 Tg yr^{-1} more than the top-down methods, primarily because of the difference in 'other natural emissions', see figure 2. Chemical reactions with OH radicals in the atmosphere are the most important sink, whereas soils are a smaller second sink (Saunois et al., 2020)

The Global Methane Budget shows how emission estimate methods can be divided into the top-down approach (atmospheric inversion or remote sensing) and the bottom-up approach (sum of individual source estimates. The difference between both approaches exemplifies the need for measurements on a local facility level. Local measurements can help facilities at estimating their own emission, and improve the comprehension of the global methane budget. But foremost, emission data on individual source levels need to be correct to realise successful short-term CH_4 emission reductions.

For this purpose, urban areas have recently been the subject of multiple campaigns. McKain et al. (2015) claim that national inventories probably underestimate urban area emissions in Boston, MA. Helfter et al. (2016) found that methane emissions in London are twice as large as documented in the national emission inventory. O'Shea et al. (2014) found that methane fluxes in Greater London are 3.4 times larger than in the emission inventory. Fossil-related emissions may be higher than currently estimated as well. Alvarez et al. (2018) found how natural gas distribution networks (NGDN) may emit up to 60% more methane than known, and Helfter et al. (2016) found NGDN to be one of the underestimated sources as well.

Maazallahi et al. (2020) recently did a methane emission assessment of street-level emissions in urban areas: the city of Utrecht (NL) and Hamburg (DE). The goal was to monitor the total emissions by NGDN gas leaks and assess the Waste Water Plant (WWTP) in Utrecht and oil and gas storage locations in Hamburg. Their campaign in Utrecht, the fourth largest city in the Netherlands, quantified total city emissions of Utrecht to be 150 +- 50 t CH_4 yr^{-1} and found the local WWTP plant to emit 160 +- 90 t yr^{-1}. When a single facility can emit as much as all leaks in the Natural Gas Distribution Networks (NDGN), getting a sense of the emissions in an industrial area such as the Port of Amsterdam with multiple CH_4-emitting facilities is highly relevant.

2.3 Inventory emissions of NL and Amsterdam

The bottom-up assembled national inventory report estimates that methane emissions in the Netherlands have decreased from 1990 to 2019 by 45%, with 0.69 Tg CH_4 emissions per year (17.2 Tg CO_2 eq.) in 2019 (Ruyssenaars et al., 2021). Agriculture (69.5%) and the waste sector (15.8%) are the largest emitters in 2019 (Ruyssenaars et al., 2021). The total reduction since 1990 can almost wholly be attributed to the decrease in the waste sector since the waste and agricultural sectors had about the same contribution to the total emissions in 1990. This reduction in the waste sector is caused by an 82.7% reduction in emissions from landfills (Ruyssenaars et al., 2021).

The emission inventory of the Amsterdam municipality level (Table 1) shows that the wastewater treatment plant (WWTP) is the biggest CH_4 emitter, emitting 25% of the municipality's total. Gas combustion and distribution are the city's second and third-largest emitters of CH_4.

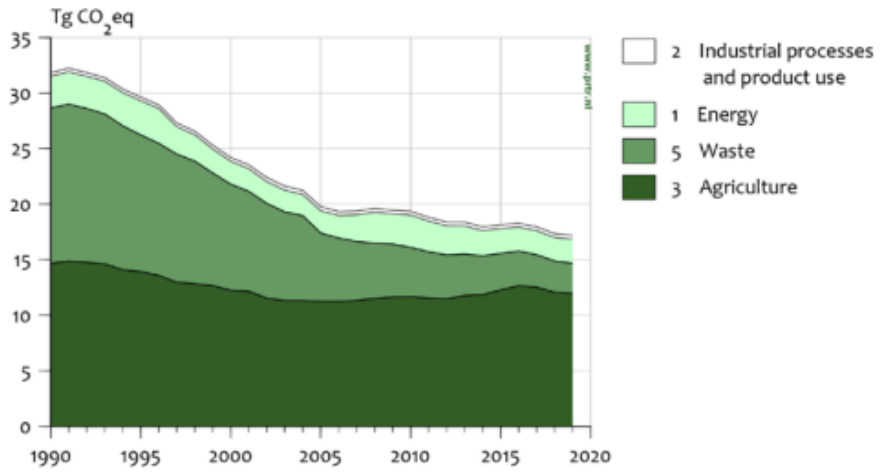

Figure 3. National total methane emissions of The Netherlands since 1990 according to the National Inventory Report 2021. Methane emissions have decreased by 45% since 1990, primarily due to the reduction in the waste sector (Ruyssenaars et al., 2021).

Table 1. The top three source categories of methane emissions in the Amsterdam municipality. According to the emission registration, the wastewater treatment facility emits about a quarter of the city's total emissions. Natural gas combustion and distribution are numbers 2 and 3 (RIVM, 2022).

Source of emission	Species	Unit	2019 Emission	% of total
WWTP emissions water and sludge line, individual (RWZI)	Methane	kg	605913	25.5%
SBI: households, combustion emissions (gas slip)	Methane	kg	459784	19.4%
Gas distribution	Methane	kg	267368	11.3%

The Port of Amsterdam, extending to the west of Amsterdam, is the second-largest port in the Netherlands and claims to be the fourth-largest port in Europe (Port of Amsterdam, 2022). The port is the 10th most CO2-emitting port in Europe, but no numbers on CH_4 emissions are known (Armstrong, 2022). With a large landfill, multiple fossil fuel storage and shipping locations, multiple wastewater treatment plants and a diverse set of other industrial facilities, this region has many possible sources of methane emission.

As all companies are obliged to register their emissions with the authorities, 12 industrial facilities were registered with methane emissions in the port of Amsterdam in 2019 (Table 2, no 1 – 12) (RIVM, 2022). The Nauerna Landfill (location no. 0) shows no registered CH_4 emissions but has been the subject of various CH_4 emission research projects and is the self-acclaimed 'best-monitored landfill of the world'. The campaigns show emission estimates between 1.5 - 3 kton CH_4 y^{-1}, making it the largest known CH_4 emitter

in the Port of Amsterdam area (Hensen, Slanina, et al., 2000; Jacobs et al., 2007). The WWTPs (locations no. 1 - 3) have the largest registered methane emissions. Their emissions together are 32 times the other registered emissions combined (RIVM, 2022).

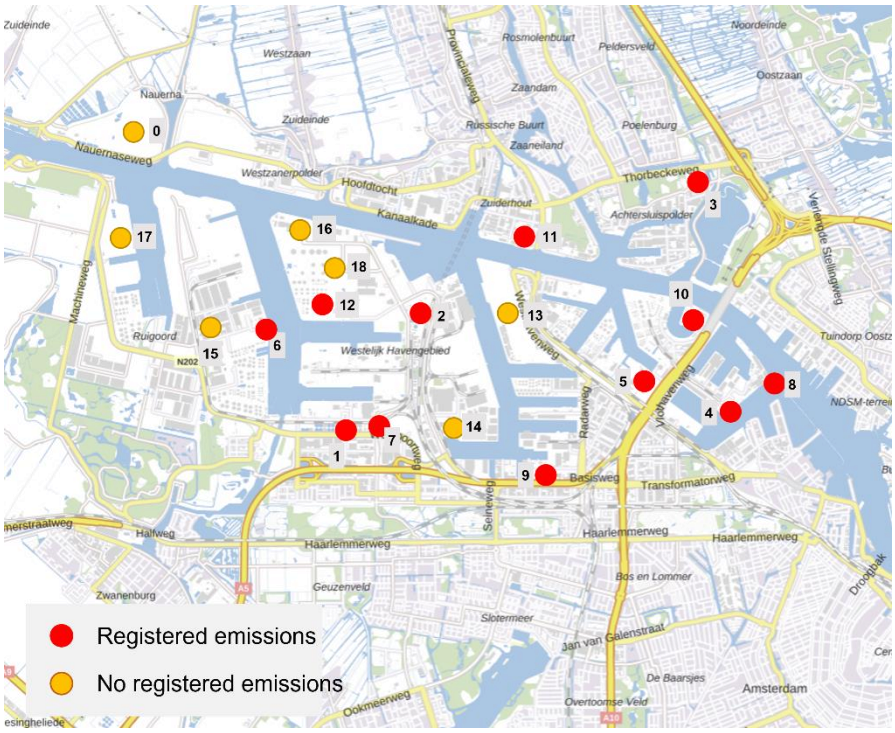

Figure 4. A map of the facilities with possible CH_4 emissions in the Port of Amsterdam region. The red symbols indicate that CH_4 emissions are registered with official authorities, the orange symbols indicate that no CH_4 emissions have been registered, but that CH_4 emissions have (possibly) been measured at earlier measurement campaigns. The description of the locations with the corresponding numbers can be found in Table 2.

Table 2. The registered 2019 methane emissions, names and descriptions of the facilities that probably emit methane in the Port of Amsterdam. The numbers correspond to the locations in Figure 4. The methane emissions are the numbers that are registered with the authorities (RIVM, 2022)

	2019 CH_4 emissions (kg)	**Company**	**Activity Description**
0	**0**	Landfill Nauerna (Afvalzorg)	A dump, recycle and storage site for building, soil and waste materials.
1	**549500**	RWZI Amsterdam-West	Wastewater treatment for Amsterdam households.
2	**59580**	RWZI Amsterdam-Westpoort	Wastewater treatment for the Port of Amsterdam industry.
3	**44390**	RWZI Zaandam-Oost	Wastewater treatment for the Zaandam households.
4	**6180**	Bunge Netherlands	Processing of soybeans.
5	**5000**	Nuon Power Generation (Hemweg)	Coal/gas energy plant, partially closed.
6	**3038**	Cargill BV	Processing of grain- and oilseeds
7	**2935**	Afval Energie Bedrijf	Processing of waste
8	**1304**	ICL Fertilizers Europe CV	Production of fertilisers and plant nutrition
9	**1138**	Sonneborn Refined Products	High-purity speciality hydrocarbons and vegetable-based emollients.
10	**590**	Main BV	Collection and storage of waste oil.
11	**131**	Cabot Norit Nederland	Producer of granular activated carbon.
12	**121**	Oxea Nederland	Producer of chemical semi-finished products.
13	**0**	OBA Terminal	Storage and transhipment terminal for coal
14	**0**	Orgaworld	Processing of organic waste, producing biogas
15	**0**	Dutch Cacao	Processing of cacao.

16	**0**	Paro Amsterdam	Processing of construction/commercial waste.
17	**0**	Rietlanden Terminals	Storage and transhipment terminal for coal
18	**0**	Vosse Groen Recycling	Collecting organic waste

2.4 Quantification models

The mass-balance approach and the Gaussian Plume Dispersion Model are the most used quantification models in CH_4 emission research projects. The mass-balance approach is based on the concept of a box, measuring the upwind influx and the downwind outflux of a trace gas. The difference between the influx and the outflux is caused by a source or multiple sources inside the box. Measuring wind speed and the mole fraction of the trace gas is needed, and this can be done with different measurement techniques (ground-based or aerial). In either method, a well-mixed boundary layer and steady horizontal winds need to be approached (Fiehn et al., 2020).

The mass-balance approach is often combined with the Gaussian Plume Dispersion Model (GPDM). In this model, a source must be assumed to be a point source, with the emissions spreading with a Gaussian distribution along the wind direction. To use this model, cross-wind transects of the plume need to be measured, which can be done by aerial or mobile approaches. Inverse modelling using the GPDM equation leads to an estimation of the point source emissions. This model can be used from a few hundred meters to 5000 meters from the source (Abdel-Rahman, 2011; Turner, 1994). The model is often used for a single source but can also be expanded to two sources (Chen et al., 2020; Lushi & Stockie, 2010).

Other quantification models are less frequently used. Abdel-Rahman (2011) claims that the Plume Rise and Dispersion Model (PRISE) should be more successful closer to the point source, but this model has not been used in any known research in the last two decades. The Lagrangian Particle Diffusion Model combines airborne and satellite data at larger spatial and temporal scales (Kort et al., 2008). Another method for larger spatial scales is simulating atmospheric transport with the FLEXible PARTicle-Weather Research and Forecasting model (FLEXPART-WRF) (Cui et al., 2015).

2.5 Measurement techniques

The quantification models can use different kinds of measurement techniques, each with different advantages. Section 2.2 divides emission approaches into bottom-up and top-down. But when speaking of measurement techniques, the division between top-down and bottom-up methods is not always clear. Therefore, it is better to divide all measurement techniques into satellite, aerial, and ground-based measurements.

2.5.1 Satellites

Satellites can measure and quantify methane emissions on local to regional scales and can cover large areas at once. The resolution is often low; therefore, it is often unable to distinguish individual sources when located close to other sources. The resolution is recently getting higher, for instance, with the TROPOspheric Monitoring Instrument (TROPOMI), which has a resolution of 7x7 km (Sadavarte et al., 2021), or the GHGSat-D satellite, with an even higher resolution of 50m x 50m (Varon et al., 2020).

2.5.2 Aerial measurements

Aircraft measurement campaigns mostly focus on identifying gas leakage in larger regions, such as larger industrial or oil and gas producing regions. Different flying strategies are used, depending on the used quantification model. When a single downwind flight transect is used, the source is often assumed to be a point source; therefore, the transect must be sufficiently far from the start (Karion et al., 2013; Turnbull et al., 2011). The approach can be expended with multiple downwind transects at different heights or horizontal distances from the source and upwind measurements as well (Fiehn et al., 2020). Circular flight paths at different heights but the same horizontal distance are also used, mainly for small point sources or small areas (Ryoo et al., 2019).

A more recent innovation in aerial measurements is using Unmanned Aerial Vehicles (UAVs or drones). UAVs are cheaper and easier to use for multiple small transects than aircraft, useful at facilities where

mobile measurements are not possible. Installing the CH_4 concentration analysers on board of an UAV for direct analysis remains a challenge for now. The samples often need transport to an analyser on the ground for analysis (Andersen et al., 2022; Gålfalk et al., 2021; Morales et al., 2021).

2.5.3 Ground-based measurements

Ground-based measurements can be divided into mobile and stationary measurements. Stationary ground measurement methods include various forms of (networks of) measurement towers, local experiments with tracer gas or other local measurements. A measurement tower can measure longer time series at the exact location. Specific equipment can be installed for longer periods when a particular site is subject to a longer emission research project, such as know emitters as landfills. (Hensen, Slanina, et al., 2000; Jacobs et al., 2007). But more importantly, worldwide networks, such as the NOAA/GML cooperative global air sampling network, are essential for measuring global trends in atmospheric methane abundance (Dlugokencky, 2021; Dlugokencky et al., 1994).

The real-time analysis of mobile measurements has proven successful in identifying and estimating facility emissions and finding fugitive gas emissions of NDGN or fossil fuel production sites in the Netherlands (Maazallahi et al., 2020; Yacovitch et al., 2015; Yacovitch et al., 2018). Mobile labs can be small and focused on measuring methane sources (Maazallahi et al., 2020) or large lorries measuring a dozen trace gasses at once (Hensen, Erisman, et al., 2000; Hensen, Slanina, et al., 2000; Jacobs et al., 2007; Scharff et al., 2003; van Dinther et al., 2021)

This method was also used at various fossil fuel locations in Groningen (NL), which were natural gas wells (Yacovitch et al., 2015; Yacovitch et al., 2018). The most recent assessment used the miniature Aerodyne Mobile Laboratory (minAML), using Tunable Infrared Laser Direct Absorption Spectroscopy (TILDAS) trace-gas monitors. This mobile lab offers real-time CH_4 and ethane (C_2H_6) monitoring to distinguish fossil from biogenic sources.

The project MEMO^2 (Methane goes Mobile – Measurements and Modeling) used and improved mobile measurements to bridge the gap between official methane emission inventories and scientific monitoring estimates. They developed new mobile measurement techniques and applied them to local methane sources throughout Europe (Walter & Röckmann, 2019).

2.6 Need for measurements

Individual facility emission numbers are often unknown or unverified, whereas they are essential for reduction strategies. A mobile measurement campaign in a larger industrial area can successfully verify the emission inventory and detect unknown CH_4 emitters. Therefore, this research aims to localise and quantify the methane emissions of the largest methane emitters in the port of Amsterdam. The amount and magnitude of the emitters in the local emission inventory will be verified with those measurements, and comparison with older measurements will give insight into trends in methane emissions.

3 Methods and Materials

3.1 Planning and Target Area

This campaign targeted 19 locations in the Port of Amsterdam area to detect the presence of CH_4 enhancement, attribute the enhancement to a source location and quantify the emission rate for this source.

Locations 1 – 12 were picked because they registered emissions with the official authorities. The locations 0 and 13 - 16 came forward in exploratory measurements by TNO with their measurement truck and were therefore also listed beforehand. The rest of the Port of Amsterdam area was also explored to find unknown emitters. Locations 17 and 18 were discovered during those exploring rounds through the area. Appendix 8.1 gives a detailed description of the facility activities, the public roads used to measure transects and the number of times each location was visited.

Each site can only be assessed with certain wind conditions; therefore, the meteorological conditions of a measurement day determined which locations were visited. Table 3 shows the wind directions for which each location could be visited.

Table 3. All the targeted facilities in the Port of Amsterdam area. For each location, the wind directions for which this facility could be visited are given.

NO	COMPANY	WIND DIRECTION
0	Landfill Nauerna	N- NNE or ESE-SE
1	RWZI Amsterdam-West	N or S
2	RWZI Amsterdam-Westpoort	SSE or W-WNW
3	RWZI Zaandam-Oost	SSE-S
4	Bunge Netherlands	ESE-SE
5	Nuon (Hemweg)	WNW-NW or N-NE
6	Cargill (Multiseed)	N-NNW
7	Afval Energie Bedrijf	N or NE
8	ICL Fertilizers Europe	E-ESE
9	Sonneborn Refined Products	N or W
10	Main BV	WNW
11	Cabot Norit Nederland	S or W
12	Oxea Nederland	N
13	OBA Terminal	WSW
14	Orgaworld	ENE or S
15	Dutch Cacao	NNW-N or W
16	Paro Amsterdam	SSW/N
17	Rietvelden Terminals	E or W
18	Vosse Groen Recycling	SW-W

During this research project, the port was visited a total of 14 times, ranging from December 2021 to May 2022. The first measurement day in (2/12/21) constituted only a visit to Landfill Nauerna, and the last day (13/05/22) was a full day of measurements at five different locations. All the other days were in February and March and were always half a day of measurements, whereas the other half of the day, the van was used for another measurement campaign in the residential parts of Amsterdam. Appendix 8.2 shows detailed information for each measurement day.

3.2 Gaussian Plume Model and methods outline

3.2.1 Gaussian Plume Model

The approach of quantifying facilities' emissions based on measurements at a distance is based on the Gaussian Plume Dispersion Model (GPDM) (Turner, 1994). This model predicts the dispersion of emissions from a point source, dependent on wind and stability parameters, therefore able to predict the emission rate at a specific distance from the source (Eq. 1). This model will be used in a reversed order, going from a measured concentration *C* at a distance from the source (x, y, z) towards the emission Q (g/s) at the estimated source location.

$$C(x,y,z) = \frac{Q}{2\,\pi\,u\,\sigma_y\,\sigma_z} \cdot \left(\exp\left(\frac{-(z - z_{source})^2}{2\,\sigma_z^2} \right) + \exp\left(\frac{-(z + z_{source})^2}{2\,\sigma_z^2} \right) \right) \cdot \exp\left(\frac{-y^2}{2 \cdot \sigma_y^2} \right) \qquad (1)$$

This equation is valid for x > 0, where x is the wind direction, y is the crosswind direction, and z is the vertical direction in meters. The diffusivity parameters σ_y and σ_z (in meters) represent the standard deviation (or width of the plume) in the y and z directions. The wind speed *u* is in m s^{-1}. In our approach, the peak of the measured concentration plume always represents the location y = 0, as it aligns with the wind direction. Therefore, the last exponential factor disappears.

3.2.2 Methods outline

The GPDM model is used to reverse model street-level mobile measurements towards methane emission numbers of specific facilities. The specifics of data collection can be read in 3.3. The driving strategy and the exact locations of measurement are described in section 3.1. The data analysis and emission quantification are described in 3.4, and section 3.5 describes the approach used to attribute the emissions to specific source locations.

3.3 Data collection and instrumentation

3.3.1 Data collection

3.3.1.1 Mobile lab set-up

All measurements were done at street level, with a mobile lab driving on public roads. The mobile lab consists of a Volkswagen van with two cavity ring-down spectroscopy (CRDS) analysers. The use of the instruments is as described in Maazallahi et al. (2020). After the first measurement day, the 2012 Volkswagen was replaced with a 2021 Volkswagen Transporter, but the measurement equipment was the same. The first CRDS analyser is of the type Picarro Inc. model G2301 and measures atmospheric mole fractions of CO_2, CH_4 and H_2O with a frequency of 0.3 Hz for each species, with a flow rate of 187 ml min^{-1} (Maazallahi et al., 2020). The second CRDS analyser is of the type Picarro Inc. model G4302, measuring the atmospheric mole fraction of C_2H_6, CH_4 and H_2O with a frequency of 1 Hz for each species. This instrument is the property of TNO and could be used during the whole project. It can be used with two settings, measuring C_2H_6 and CH_4, or CH_4 only. In this campaign, the setting of measuring both species was used. In this mode, the reproducibility for CH_4 is 100 ppb, and for C_2H_6 is 15 ppb. The G4302 has a cell volume of 35 mL and a flow rate of 2.2 L min^{-1}, refreshing the cell every 0.001 s. The inlet to both analysers is in the van's front bumper, about 90 cm above street level.

Both CRDS analysers were placed on the backseats of the van. They both have an interface showing the measured values in real-time, but only the G4302 interface was in front of the passenger seat. Therefore the G4302 measurements (having a higher frequency) were mainly directive in the live detection of methane plumes. The GPS recording was done with a GPS Logger app on a dedicated Samsung mobile device and a personal mobile device as backup.

3.3.1.2 Delay times

At the start of a measurement day, the UTC delays between the GPS and CRDS instruments were determined for time correction. Also, the delay between the gas inlet and the CRDS signal was determined by breathing into the inlet at specific times and calculating the time difference to the peak of the CRDS signal. Because the internal clock of the equipment was not calibrated perfectly, this difference could increase every day until it was connected to the internet and calibrated again.

3.3.1.3 Detection and Transects

One to five of the 19 locations were visited on a measurement day, depending on the time availability and the wind direction. When a CH4 plume was encountered, a minimum of 10 transects was measured. A successful transect is approximately perpendicular to the wind direction and has the van driving between 25 and 50 km/h without any stops. Also, the road must be long enough on both sides of the peak to record the full plume, including the background before and after the peak.

The measurement instruments were running and measuring continuously during the whole day. Therefore, each transect's beginning and end times were noted (in UTC) and afterwards digitalised to be read by the python script. Any remark, such as stops, weather changes, possible unknown sources or other influences on the measurements were also noted.

3.3.2 Meteorological data

Meteorological information could not be obtained from weather stations within the Port of Amsterdam area, and the closest stations were too far to rely on. Therefore, data from the Weather Research and Forecasting (WRF) model was used (Skamarock et al., 2019). This model assimilates data from KNMI meteorological measurements at their weather stations for numerical weather prediction at a 0.02° x 0.02°

scale and hourly frequency. It has 20 different layers, of which the bottom layer was used. For the measurement days, this model was used to predict the 52.40° – 52.44°, 4.74° – 4.86° area, which covers the whole port of Amsterdam. The data was hourly averaged as needed for the GPDM (Bailey, 2000). A 15% uncertainty range was assumed on the WRF model data (Fernández-González et al., 2018).

As the model was temporarily down in May 2022, observations from KNMI station Schiphol (52.32N, 4.79E) were used for the measurements on May 13th. This is the closest KNMI station to the port area, at roughly 9 km. This data was also retrieved for the other measurement days to compare the influence of the meteorological data. The model area and the location of the KNMI station are shown in Figure 5.

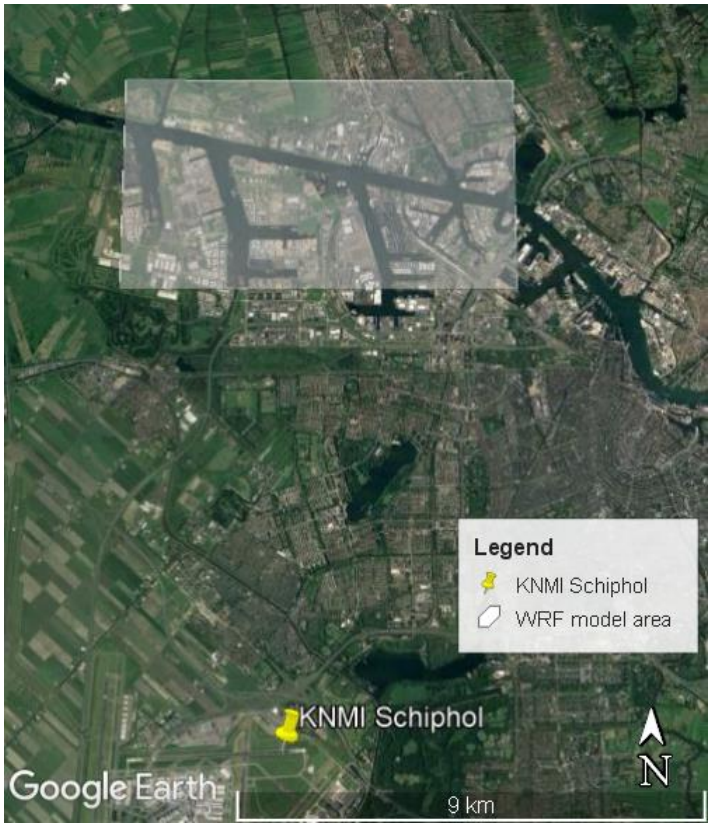

Figure 5. A map of the port of Amsterdam area with the KNMI measurement station at Schiphol roughly 9 km to the south of the port. The white rectangle shows the 52.40° – 52.44°, 4.74° – 4.86° area, over which the WRF model results are averaged and used.

3.4 Emission Quantification

3.4.1 Data preparation and background extraction of mobile measurements

The data had to be merged and adjusted to prepare for the data analysis. Data manipulation and analysis were done with Python in the Spyder editor (running on Windows). A measurement day resulted in three different output files: the GPS data, Picarro G2301 and Picarro 4302 output files. The noted delay time for the measurement data was subtracted, so the GPS and data files could be merged and interpolated. The Picarro G2301 and the Picarro G4302 were calibrated using the method from Maazallahi et al. (2020), shown in Appendix 8.3: equations 1-4.

In a 10-minute rolling window, the 25th percentile was chosen as the background value to extract the concentration enhancement for methane and carbon dioxide. This was subtracted from the measurements to obtain the elevation above the background level. For the G4302 ethane with more substantial noise fluctuations and fewer peaks, the background was chosen in the middle of the noise range, at the 50th percentile in a 10-minute rolling window. And because of a large amount of noise, a threshold of 10 ppb was chosen, below which all data were seen as noise and set to zero. The range of the noise was selected as the measurement error and was determined as the difference between the 1st percentile and the background (the 25th percentile).

3.4.2 Quantification of methane emissions

3.4.2.1 Transect Quality Check

The noted transect times were used to extract the data and create a figure and kml file for each transect to perform a quality check that consisted of 3 steps.

The first check is the Picarro alarm status being zero (Figure 7, upper panel). Secondly, the G2301 and G4302 peaks sometimes weren't exactly overlapping, indicating that the time delay needed an extra adjustment to shift the peaks to the same time. Thirdly, the peak needs to be in the middle of the transect for optimal fitting of a Gaussian shape. Therefore, the transects needed to be shortened and centred around the peak by manually adjusting the start and end times whilst maintaining a constant speed of the car during the whole transect. Lastly, the transect needed a qualitative judgement in Google Earth to check that the GPS logger recorded the track precisely on the correct road.

3.4.2.2 Gaussian fit

When a transect passed the quality check, a gaussian function $\left(A * e^{-\frac{(x-x_0)^2}{2\sigma^2}}\right)$ was fitted to the data of the CH_4 peak, using a curve fitting function of the SciPy package in Python. This fit resulted in a new maximum elevation value (A), and a sigma (σ) value for the width of the fit, corresponding to σ_y in the GPDM. The maximum of this Gaussian fit, determines the direction of the x-axis ($y = 0$). Using the estimated location of the source. This location also determines the horizontal and vertical distance x, z from the peak to the source. The maximum value (A) of the Gaussian fit is converted from mixing ratio ppm to g/m^3 to be used as the enhanced concentration in the GDPM quantification, using equation 2, with pressure (P), molecular mass (M), ideal gas constant (R) and temperature (T).

$$C\left[\frac{g}{m^3}\right] = \frac{P * M * \chi\,[ppm]}{\left(R * (273.2 + T)\right)} \quad (2)$$

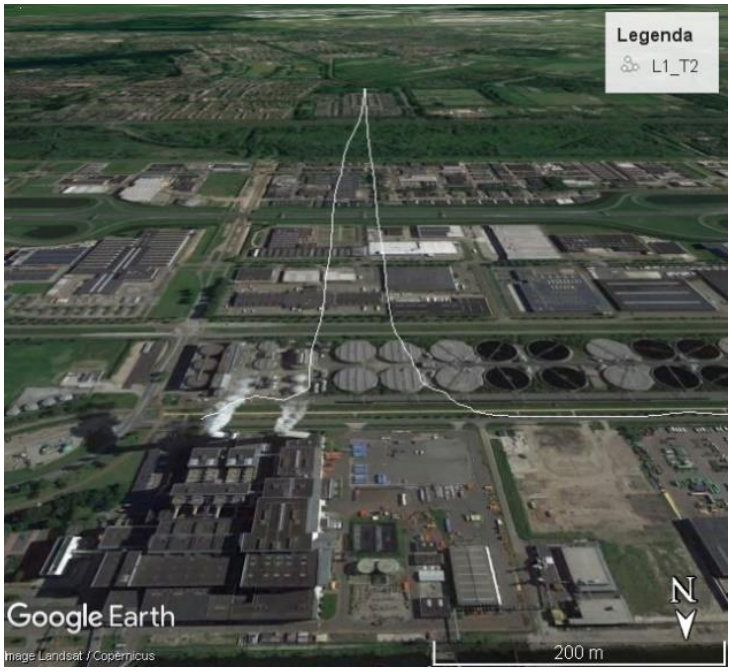

Figure 6. An individual transect visualisation at WWT Amsterdam West (1) in Google Earth.

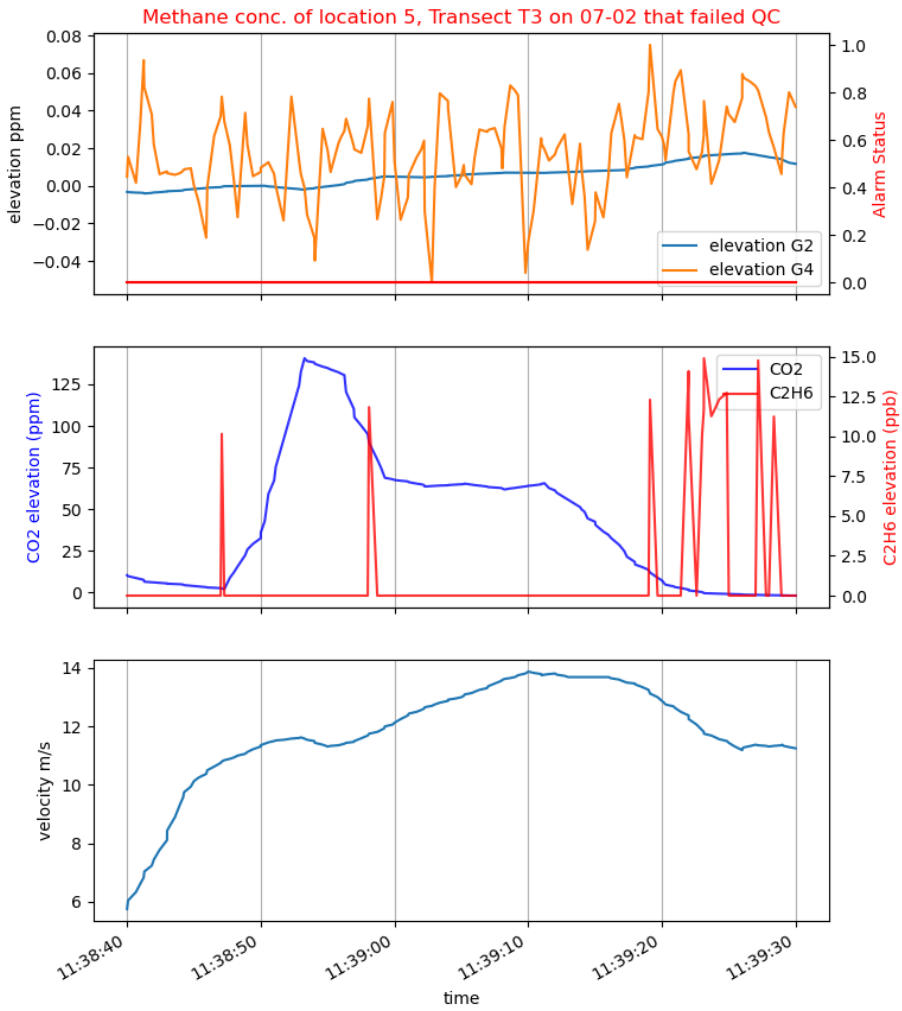

Figure 7. The panels that are used to check the quality of a transect. The x-axis of all three panels is the same as an individual transect's timeframe. In this case, the G2301 methane measurement passed the quality check, and the Gaussian fit to the plume is shown in the upper panel. The upper panel shows the methane elevation by the Picarro G2301 and G4302 (G2301: blue, G4302: orange, scale: left y-axis), together with the alarm status (red, right y-axis). The middle axis shows the CO_2 (blue, left axis) and C_2H_6 (red, right axis) recordings, which can be used to attribute the source of the methane. The bottom panel shows the speed of the car during the whole transect.

3.4.2.3 Stability Class determination

From the meteorological data, the wind speed and incoming shortwave radiation were used to determine the Pasquill-Gifford stability class, which is needed for the Gaussian Plume Model. For each transect, the time in the middle was used to find the accessory interpolated meteorological data to calculate the stability class. The categorisation comes from Bailey (2000) and is shown in Table 4. This was done for the Schiphol measurements and the WRF model data separately to compare the results and evaluate the sensitivity of using the two different datasets.

Table 4. Table 6-7 in Bailey (2000). This table determines the boundary layer stability category based on wind speed and incoming short wave solar radiation intensity. Those parameters were used to calculate the emissions values.

Key to Solar Radiation Delta-T (SRDT) Method for Estimating Pasquill-Gifford (P-G) Stability Categories

DAYTIME				
	Solar Radiation (W/m^2)			
Wind Speed (m/s)	≥ 925	925 - 675	675 - 175	< 175
< 2	A	A	B	D
2 - 3	A	B	C	D
3 - 5	B	B	C	D
5 - 6	C	C	D	D
≥ 6	C	D	D	D

The resulting stability class, combined with the distance from source to peak x, is used to calculate a theoretical value for the horizontal and vertical plume dispersion coefficients σ_y and σ_z. The vertical coefficient σ_z is calculated as in eq. 3, where *a* and *b* are parameters based on the stability class. This theoretical σ_z is used for quantification of the emissions in the GDPM. The theoretical σ_y is only used to compare with the observed σ_y., This parameter is calculated as in equations 4/5, with c and d, determined using the stability class. The difference between the calculated and observed values is used as the uncertainty for σ_z.

$$\sigma_z = a \cdot \mathrm{x}^b \tag{3}$$

$$\sigma_y = 465.11628 \cdot x \cdot \tan(\Theta) \tag{4}$$

$$\Theta = 0.017453293 \cdot \left(c - d \cdot \ln(\mathrm{x})\right) \tag{5}$$

3.4.2.4 Quantification

Using a rearranged version of eq. 1, the emissions are calculated as in equation 6.

$$Q\ [\mathrm{g\ s^{-1}}] = \mathrm{C}\ \frac{\left(2\ \pi\ \mathrm{u}\ \sigma_y \sigma_z\right)}{2\exp\left((-1)\cdot\frac{(y)^2}{2\ {\sigma_z}^2}\right)} \tag{6}$$

Because the variability of emissions might significantly influence the results, the emission rate was reported in kg/hour. All results are showcased in these units, and yearly registered emissions are downscaled to these units for comparison. A flowchart of all method steps is given in Appendix 2.

The quantification was done with 4 combinations of the Picarro analysers (G2301 and G4302) and the meteorological datasets (WRF model and Schiphol observations). Therefore, each transect resulted in 4 emission rates with an uncertainty range. Consequently, averaging the transect emission rates for each method resulted in 4 averaged emission rates (with uncertainty range) for each location.

A distance threshold was introduced to exclude measurements that are too close to the source. This threshold is different per location because it was defined as *5 dx* (the uncertainty in the along-wind distance). If part of the measurements passed this threshold, the average emission rates were calculated with those measurements only. If no measurements passed the threshold, the average rates were calculated with the measurements below the threshold.

3.5 Emission Attribution

The assumed point source location, height and corresponding uncertainties in x and z are chosen manually, based on satellite images of the facility and the expected source location. The reasoning per location is explained in 8.1.

The measurements of C_2H_6 and CO_2 were used to attribute the emission sources. This was done during driving, mainly to exclude car combustion emissions, and afterwards, to compare with the expectation of the source type, e.g. microbial emission from the WWTP or fossil emissions from the coal transhipment terminals.

4 Results

4.1 Overview

Not all locations could be measured or quantified in this project due to meteorological conditions and the availability of public roads around the facility. Figure 8 and Table 5 show to what extent each location's emissions could be verified. After 14 different days, methane emissions were detected at 12 out of 19 locations in the Port of Amsterdam area. At six locations (no 8 – 12 & 16), we could not come close enough to detect emissions or confidently claim that we did not measure any emissions. At Nuon Hemweg (loc. 5), we did three days with transects to conclude that we did not detect any emissions.

In this chapter, Section 4.2 will describe the detailed results for each location. Section 4.3 gives an overview of all locations, and section 4.4 compares the two meteorological datasets used in the model.

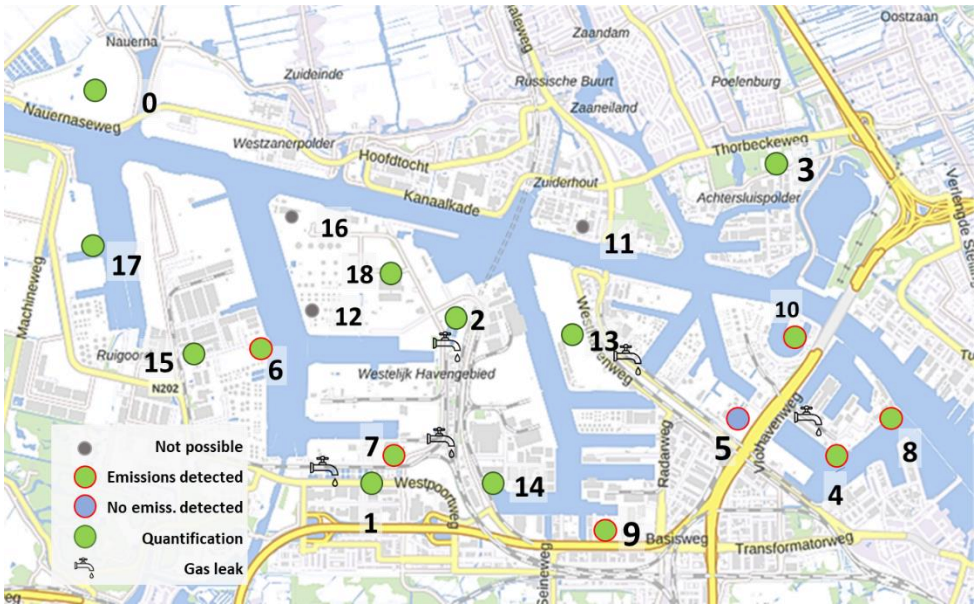

Figure 8. This map shows an overview of all facilities of interest in the port area and to what extent methane emissions could be detected and quantified. Own adaptation of map from OpenStreetMap.

Table 5. An overview of the results per location. The second column indicates the detection of a methane plume that could be attributed to the facility. 'Not possible' means it was impossible to get close enough on a public road with any wind direction. 'Yes' means that methane enhancements were detected. In this case, the next column indicates if successful transects were possible and how many days with successful transects were completed.

	NAME	EMISSIONS DETECTED	QUANTIF.	DAYS WITH TRANSECTS
0	Landfill Nauerna	Yes	Yes	4
1	RWZI Amsterdam-West	Yes	Yes	2
2	RWZI Amsterdam-Westpoort	Yes	Yes	2
3	RWZI Zaandam-Oost	Yes	Yes	1
4	Bunge Netherlands	Yes	Not possible	
5	Nuon (Hemweg)	Not possible	-	-
6	Cargill	Yes	Not possible	-
7	Afval Energie Bedrijf	Yes	Not possible	-
8	ICL Fertilizers Europe	Not possible	-	-
9	Sonneborn Refined Products	Not possible	-	-
10	Main BV (Amsterdam)	Not possible	-	-
11	Cabot Norit Nederland	Not possible	-	-
12	Oxea Nederland	Not possible	-	-
13	OBA Terminal	Yes	Yes	7
14	Orgaworld	Yes	Yes	4
15	Dutch Cacao	Yes	Yes	3
16	Paro Amsterdam	Not possible	-	-
17	Rietlanden Terminals	Yes	Yes	4
18	Vosse Groen Recyling	Yes	Yes	2

4.2 Individual Locations

For all quantified locations, this section shows a graph with the transects' emission rates for the method using the combination of the Picarro G2301 analyser and the WRF model meteorological data (from now on: G2301/WRF method), shown at a distance to the source. The graph also shows the averages for the four combinations of methods (see 3.4.2.4) and the expected or registered emission rates if they were provided.

4.2.1 Location 0: Landfill Nauerna (Waste)

Figure 9 shows the emission rates for individual transects at Landfill Nauerna, using the G2301/WRF method. It shows 2 distinct groups of measurements, where the first group consists of measurements at 2 different roads (see appendix 8.1.1). The second group is at roughly twice the distance of the first group and is measured at a third road. The figure shows that the measurements the closest to the source generally result in the highest emission rates. The emission rates decrease as the distance increases, but the emission rates of the second group are similar to the last 8 measurements of the first group. Although this facility's CH_4 emissions have been measured in earlier campaigns, they are not registered in national inventory. The results of the most recent campaign is shown at 172.8 kg CH_4 h^{-1}.

The threshold of 750 meters excludes all measurements of the first group of measurements. The highest and lowest individual emission estimates shown are both below the distance threshold: 785.5 ± 1080.5 kg CH_4 h^{-1} at 338 meters distance and 19.1 ± 11.5 kg CH_4 h^{-1} at 612 meters distance. When the measurements below the threshold are excluded, the highest emission rate is 173.3 ± 140.4 kg CH_4 h^{-1} at 981 meters, and the lowest emission rate is 67.7 ± 25.1 kg CH_4 h^{-1} at 938 meters distance.

The expected emission rate is 171.2 kg CH_4 h^{-1} and is based on an earlier measurement campaign (Jacobs et al., 2007). The average values are well below the expected emission rate. The Schiphol method gives the emission rates 88.3 ± 10.6 kg CH_4 h^{-1} (G2301) and 91.4 ± 12.1 kg CH_4 h^{-1} (G4301). The WRF method shows higher averages: 102.1 ± 26.0 kg CH_4 h^{-1} (G2301) and 105.7 ± 14 kg CH_4 h^{-1} (G4302). The Picarro G4302 and WRF model data combination results in the highest average emission rate.

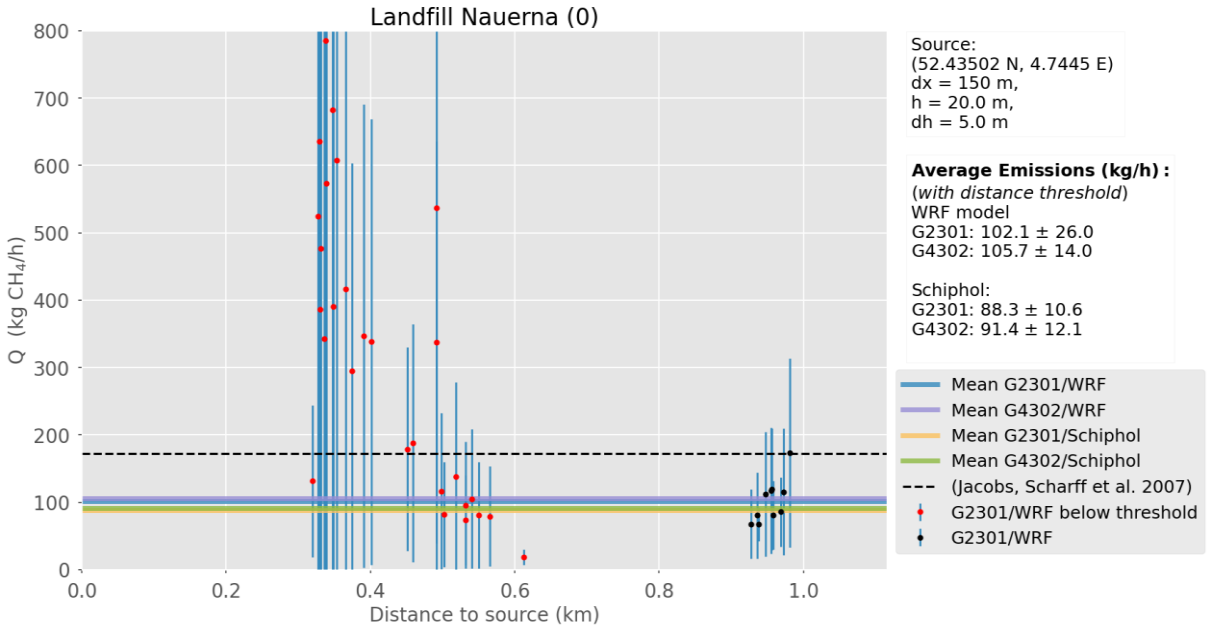

Figure 9. The quantified emission rates at Landfill Nauerna. The individual transect emission rates for the Picarro G2301 and WRF meteorological data method are displaced at the measurement's estimated distance to the point source location. The Schiphol estimates average is about 10% lower than the WRF averages. The highest average emission rate is from the G4302/WRF method, at 105.7 ±14.0 kg CH_4 h^{-1}. The distribution shows that measurements at short distances give high results, but as the distance increases, the emission results stabilise.

4.2.2 Location 1: Wastewater Treatment Amsterdam West (WWTP)

Figure 10 shows all individual emission rate estimates using the G2301/WRF method. It shows that all the transects downwind the WWTP Amsterdam West are at roughly 125 meters from the source because only one road was used for transects. The distance uncertainty at this location is defined as 30 meters, and the closest measurements are below 150 meters. Therefore, applying the distance threshold to this location excludes all measurements.

The emission rates in the shown group of measurements range between a minimum of 5.0 ± 4.1 kg CH_4 h^{-1} at 112 meters distance and a maximum of 53.9 ± 37.9 kg CH_4 h^{-1} at 124 meters distance. The combination of the Picarro G2301 and Schiphol meteorological data gives the highest emission rate, but all averages are similar and within each other's uncertainty range. The WRF model method results in 24.8 ± 4.8 kg CH_4 h^{-1} (G2301) and 23.9 ± 2.4 kg CH_4 h^{-1} (G4302). The Schiphol method results in 25.6 ± 2.6 (G2301) and 24.4 ± 2.5 kg CH_4 h^{-1} (G4302). The registered amount of emissions is for each method's average outside the uncertainty range. With 62.7 kg CH_4 h^{-1}, the registered amount of emissions is about 2.5 times larger than the average values. This registered value is outside the average uncertainty range for each method.

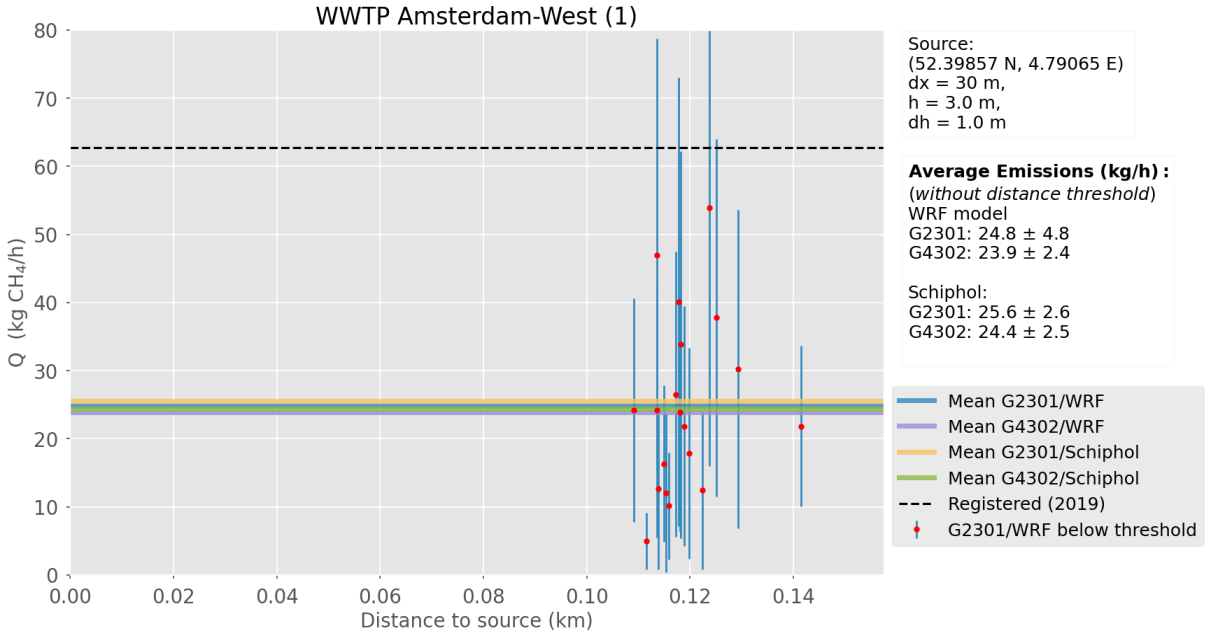

Figure 10. For WWTP Amsterdam-West, this figure shows the calculated methane emission rates (kg CH_4 h^{-1}) based on G2301/WRF method at a given distance to the assumed source (km). There is one set of measurements at roughly 120 meters from the source. The four averages are between 23.9 ± 2.4 kg CH_4 h^{-1} and 25.6 ± 2.6 kg CH_4 h^{-1}. The 2019 registered amount of emissions is 62.7 kg CH_4 h^{-1}, which is well above average.

4.2.3 Location 2: Wastewater Treatment Amsterdam Westpoort (WWTP)

The methane peaks downwind of WWTP Amsterdam Westpoort are measured at roughly 225 – 425 meters from the source, all along the same road section that curves around the WWTP (see appendix 8.1.3). Figure 11 shows the emission rates for this group of measurements using the G2301/WRF method. The distance threshold at this location is defined as 200 meters, so none of the measurements is excluded by this threshold.

The highest individual emission rate in the figure is 32.6 ± 17.4 kg CH_4 h^{-1} at 404 meters distance. The lowest emission rate is 9.9 ± 8.1 kg CH_4 h^{-1} at 301 meters distance. The WRF meteorological method clearly shows higher average emission rates than the Schiphol method, with almost a factor 2 difference. The Picarro G4302/WRF meteorological data combination gives the highest average emission rate. The WRF method averages are 17.6 ± 3.0 kg CH_4 h^{-1} (G2301) and 19.6 ± 2.5 kg CH_4 h^{-1} (G4302), whereas the averages are 9.9 ± 0.7 kg CH_4 h^{-1} (G2301) and 11.4 ± 1.4 kg CH_4 h^{-1} (G4302) for the Schiphol method. The registered amount of emissions, which is 6.8 kg CH_4 h^{-1}, is below and outside the uncertainty ranges of all the average values.

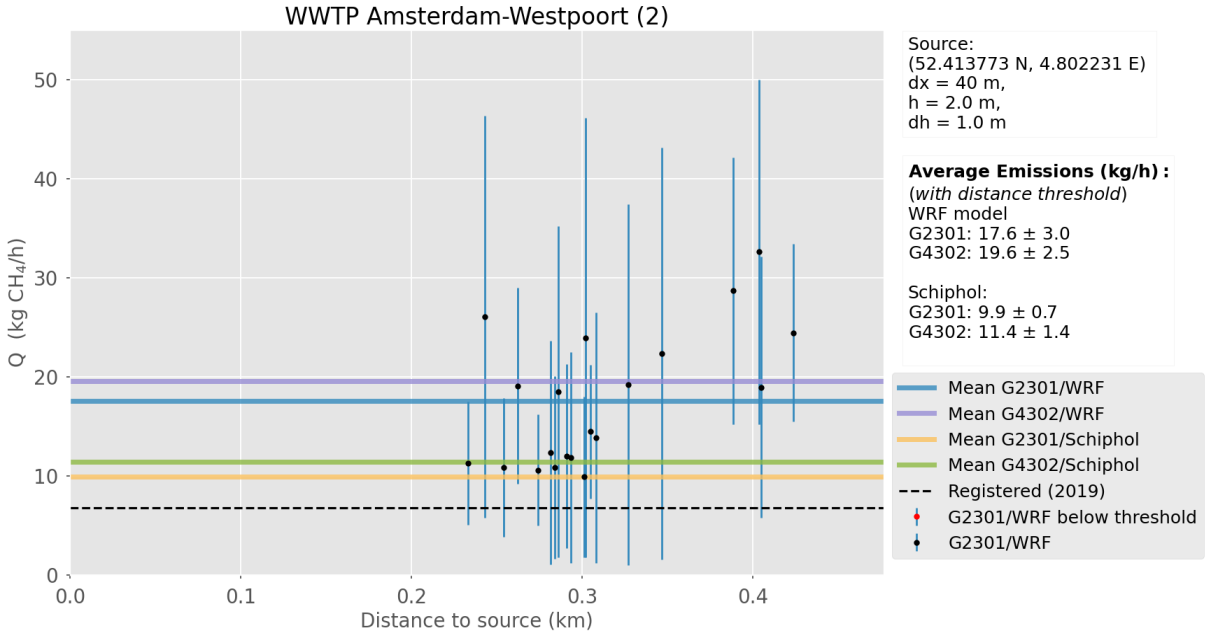

Figure 11. This figure shows the calculated methane emission rates (kg CH_4 h^{-1}) based on G2301/WRF measurements at a distance to the source (km) for WWTP Amsterdam Westpoort. The individual transect emission rates for the G2301 results are shown, which range between 10 ± 8 kg CH_4 h^{-1} and 33 ± 17 kg CH_4 h^{-1}. The averages of the four different methods are shown as horizontal lines, ranging between 9.9 ± 0.7 kg CH_4 h^{-1} (G2301/Schiphol) and 19.6 ± 2.5 kg CH_4 h^{-1}. On average, the WRF method results are higher than the Schiphol method results. All averages are above the number of registered emissions in 2019.

4.2.4 Location 3: Wastewater Treatment Zaandam-Oost (WWTP)

The estimated emissions of WWTP Zaandam-Oost are based on one day of measurements, with all transects on the same road. Figure 12 shows the individual transect results for the G2301/WRF method at a distance of 65 – 130 meters to the source. This location's distance threshold is defined as 200 meters, which would exclude all measurements. Therefore, the four averages in Figure 12 are calculated without the distance threshold.

The individual transects range between 4.0 ± 4.3 kg CH_4 h^{-1} at 66 meters and 7.6 kg ± 8.1 CH_4 h^{-1} at 72 meters distance. For each Picarro instrument, the WRF method result is higher than the Schiphol result. The Picarro G2301/WRF model combination gives the highest average of 5.3 ± 1.6 kg CH_4 h^{-1}, followed by the G2301/Schiphol combination with 4.9 ± 0.8 kg CH_4 h^{-1}. The other average values are within the uncertainty range of these two, at 4.8 ± 0.8 kg CH_4 h^{-1} (G4302/WRF) and 4.4 ± 0.8 kg CH_4 h^{-1} (G4302/Schiphol). The registered amount of emissions is 5.1 kg CH_4 h^{-1}, which is within the uncertainty range of all four averages.

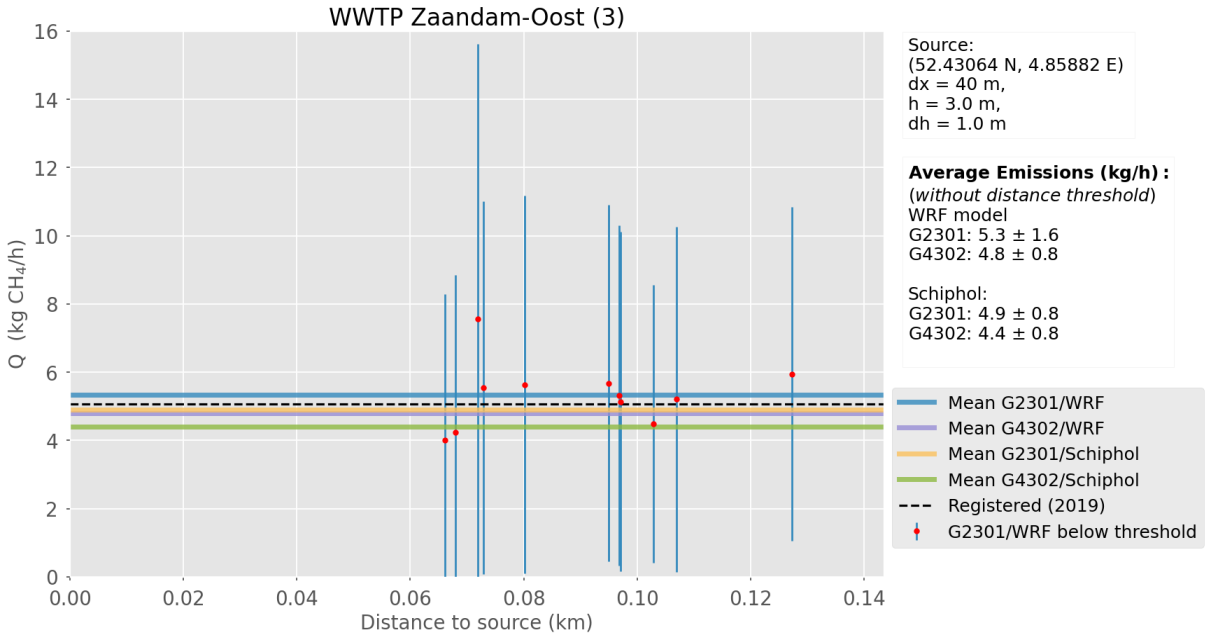

Figure 12. This figure shows the calculated methane emission rates (kg CH_4 h^{-1}) based on G2301/WRF measurements at a distance to the source (km) for WWT Zaandam Oost. The individual transect emission rates for the G2301 results are shown, and the averages of all result categories are shown as horizontal lines. The figure shows how all result averages are close to each other, within the range of uncertainty of the highest average value 5.3 ± 1.6 kg CH_4 h^{-1}. The registered emission rate of 5.1 kg CH_4 h^{-1} is also in this uncertainty range.

4.2.5 Location 13: OBA Terminal (Energy)

The measurements downwind of the OBA Terminal were done on three different roads. Figure 13 shows the individual measurements for the G2301/WRF method, with 2 distinct groups of measurements. The first group consists of measurements at 2 different roads. The second group, starting at 1200 meters distance, was measured across a waterway (see Appendix 8.1.14). The distance threshold of this location is defined as 400 meters, which excludes half of the first group of measurements.

The highest emission rate estimate is 510.7 ± 1151.3 kg CH_4 h^{-1}, measured at 205 meters distance and is one of the excluded measurements. After implementing the distance threshold, the highest individual emission rate is 482.2 ± 300.0 kg CH_4 h^{-1} at 1245 meters distance. The lowest emission rate is 7.1 ± 4.7 kg CH_4 h^{-1}, of which the peak was measured at 1200 meters distance. The Picarro G4302/WRF model combination gives the highest average emission rate: 83.1 ± 8.2 kg CH_4 h^{-1}. The G2301/WRF combination is similar, at 79.4 ± 12.3 kg CH_4 h^{-1}. The Schiphol method averages are lower, at 74.9 ± 7.1 kg CH_4 h^{-1} (G4302) and 71.9 ± 6.2 kg CH_4 h^{-1} (G2301). This location had no registered CH_4 emissions.

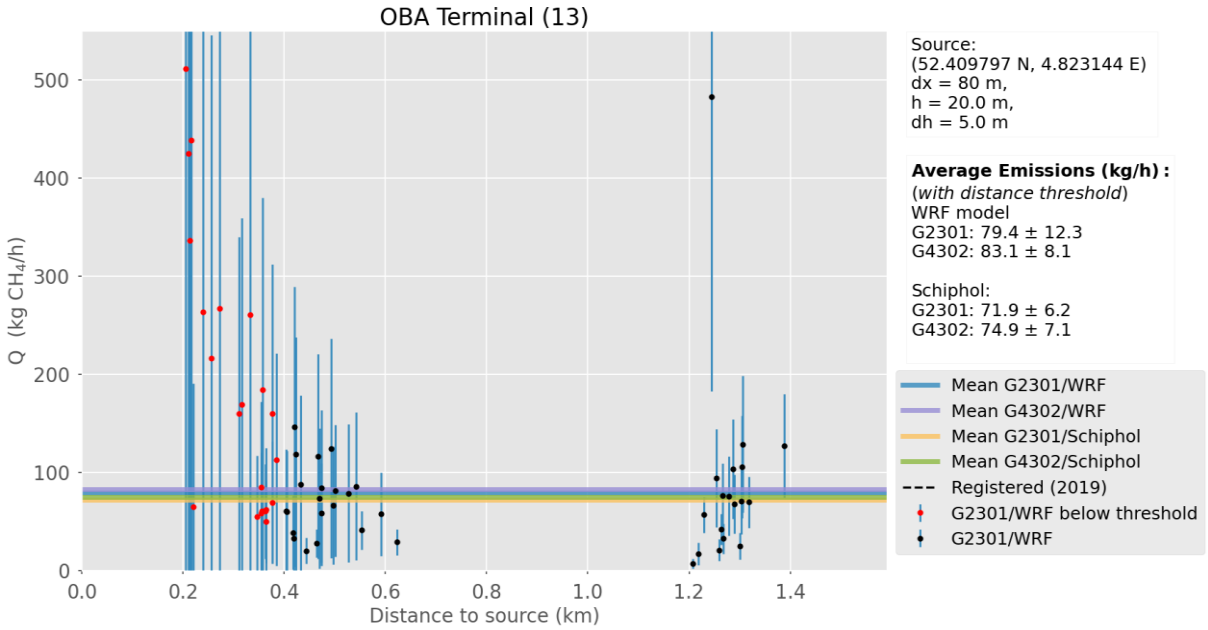

Figure 13. This figure shows the calculated methane emission rates (kg CH_4 h^{-1}) based on G2301/WRF measurements at a distance to the source (km) for the OBA Terminal. The measurement distance to the source ranges from 200 to 1400 meters. The average difference between the meteorological result groups is larger than the average difference between the two Picarro instruments. The highest average rate is 83.1 ± 8.2 kg CH_4 h^{-1}, which is from the G4302/WRF method. This facility had no registered methane emissions.

4.2.6 Location 14: Orgaworld (Energy/Waste)

All transects at Orgaworld were done on the same road, at a minimum of 300 meters to the source. This means that measurements at a greater distance, as shown in Figure 14, aren't more reliable because they result in a smaller angle between the wind and the road. The distance threshold is defined as 300 meters, which excludes 5 measurements.

The individual emission estimates that are shown in Figure 14 range between a minimum of 3.4 ± 1.1 kg CH_4 h^{-1} at 414 meters distance and a maximum of 30.7 ± 18.9 kg CH_4 h^{-1} at 304 meters distance.

The G2301/WRF method gives the highest average emission rate, 10.6 ± 1.8 kg CH_4 h^{-1}. The other averages fall within this uncertainty range. The G4302/WRF method gives an average of 10.2 ± 1.0 kg CH_4 h^{-1}, and the Schiphol method gives averages of 10.0 ± 0.9 kg CH_4 h^{-1} (G2301) and 9.7 ± 0.9 kg CH_4 h^{-1} (G4302). This location had no emissions registered.

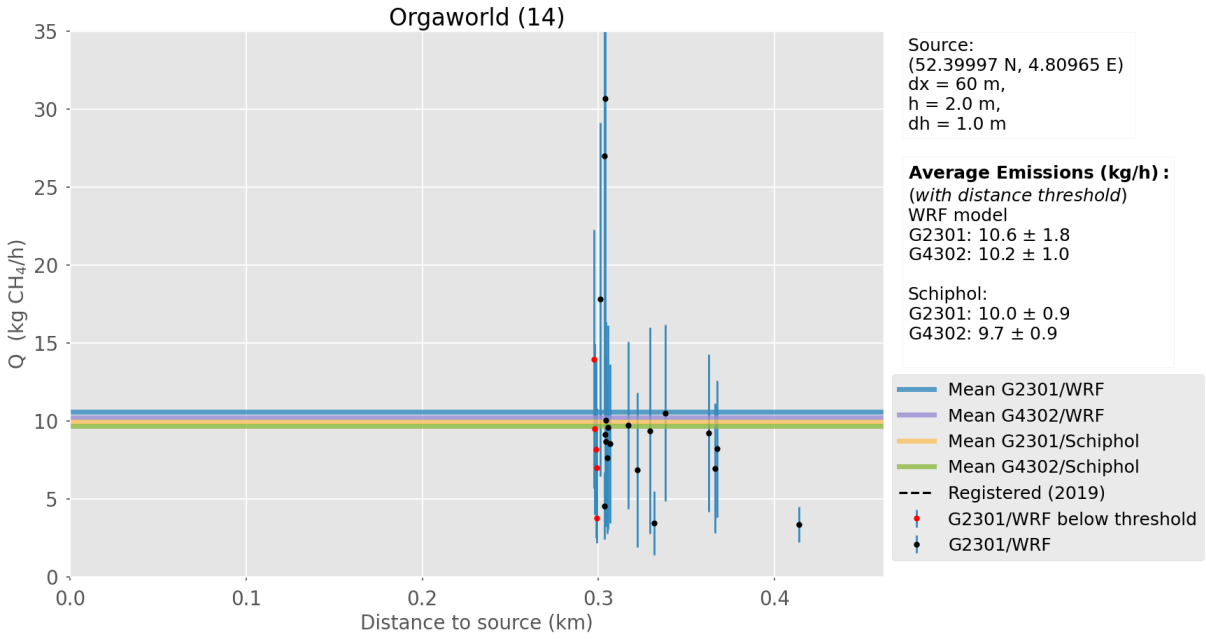

Figure 14. This figure shows the calculated G2301/WRF emission rates based on measurements on one road, approximately 300 meters from the source. The averages of the four approaches are similar, around 10 kg CH_4 h^{-1}, and the highest average emission rate of 10.6 ± 1.8 kg CH_4 h^{-1} is found using the G2301/WRF method. Still, the other averages fall within its range of uncertainty. The highest G2301/WRF emission rate is 30.7 ± 18.9 kg CH_4 h^{-1} at 304 meters. The lowest rate is 3.4 ± 1.1 kg CH_4 h^{-1}, at 414 meters. This facility had no emissions registered.

4.2.7 Location 15: Dutch Cacao (Food)

Out of a total of 56 transects, the 15 transects that passed the quality check for Dutch Cacao are shown in Figure 15. All measurements are roughly 400 meters from the source, whereas measurements at a smaller distance didn't show any CH_4 concentration peaks (see appendix 8.1.16). The distance threshold is defined as 50 meters and does not exclude any measurements.

The individual emission estimates shown (using the WRF/G2301 method) range between 16.6 ± 18.7 kg CH_4 h^{-1} at 397 meters distance and 123.3 ± 122.9 at 384 meters distance. The G4302/WRF method shows the highest average emission rate of 74.1 ± 32.2 kg CH_4 h^{-1} and the G2301/WRF method follows at 59.0 ± 17.2 kg CH_4 h^{-1}. The Schiphol method gives lower averages of 50.8 ± 23.1 kg CH_4 h^{-1} (G4302) and 38.9 ± 10.1 kg CH_4 h^{-1} (G2301). This difference between the methods is large compared to other facilities. The averages also show relatively large uncertainty ranges. This facility had no CH_4 emissions registered.

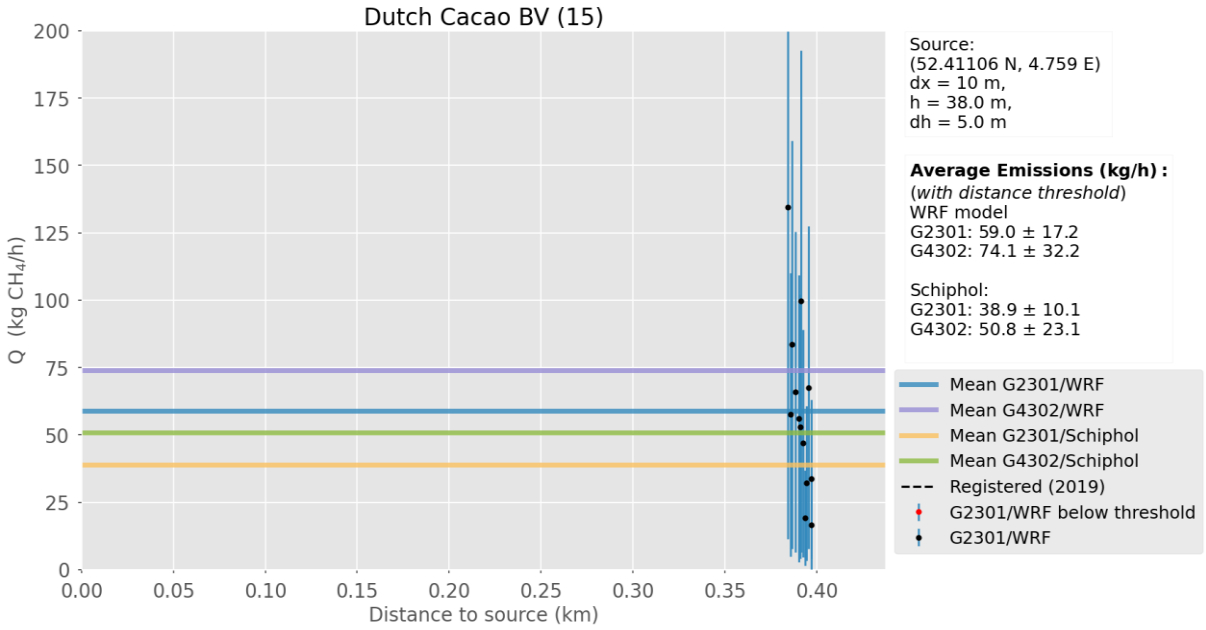

Figure 15. The emission rates for the Dutch Cacao facility. The individual emissions rates of the G2301/WRF method are shown in this figure, together with the average emission rates of all four approaches. All measurements are conducted on the same road, and the most significant difference in distance to the source is less than 15 meters. This location has substantial differences between the Picarro instruments and between the meteorological methods, with averages ranging between 38.9 ± 10.1 kg CH_4 h^{-1} for the G2301/Schiphol method and 74.1 ± 32.2 kg CH_4 h^{-1} for the G4302/WRF method.

4.2.8 Location 17: Rietlanden Terminal (Energy)

The results for the Rietlanden Terminal are shown in Figure 16. The figure shows two groups of measurements, of which the furthest group was measured across a waterway. The distance threshold is defined as 500 meters and excludes the first group of measurements.

The first group with the closest measurements gives the highest emission rates, with a maximum of 157.7 ± 199.3 kg CH_4 h^{-1} at 384 meters. The second group of measurements is measured at over twice the distance across a waterway and has lower emission rates. The highest emission rate in this group is 53.0 ± 37.5 kg CH_4 h^{-1} at 851 meters distance, and the lowest emission rate is 204 ± 7.2 kg CH_4 h^{-1} at 830 meters distance.

The WRF method gives the highest averages of 35.2 ± 8.2 kg CH_4 h^{-1} (G4302) and 32.1 ± 7.2 kg CH_4 h^{-1} (G2301). The Schiphol averages are below these uncertainty ranges, at 20.4 ± 2.4 kg CH_4 h^{-1} (G2301) and 22.3 ± 5.3 kg CH_4 h^{-1}. This facility had no emissions registered.

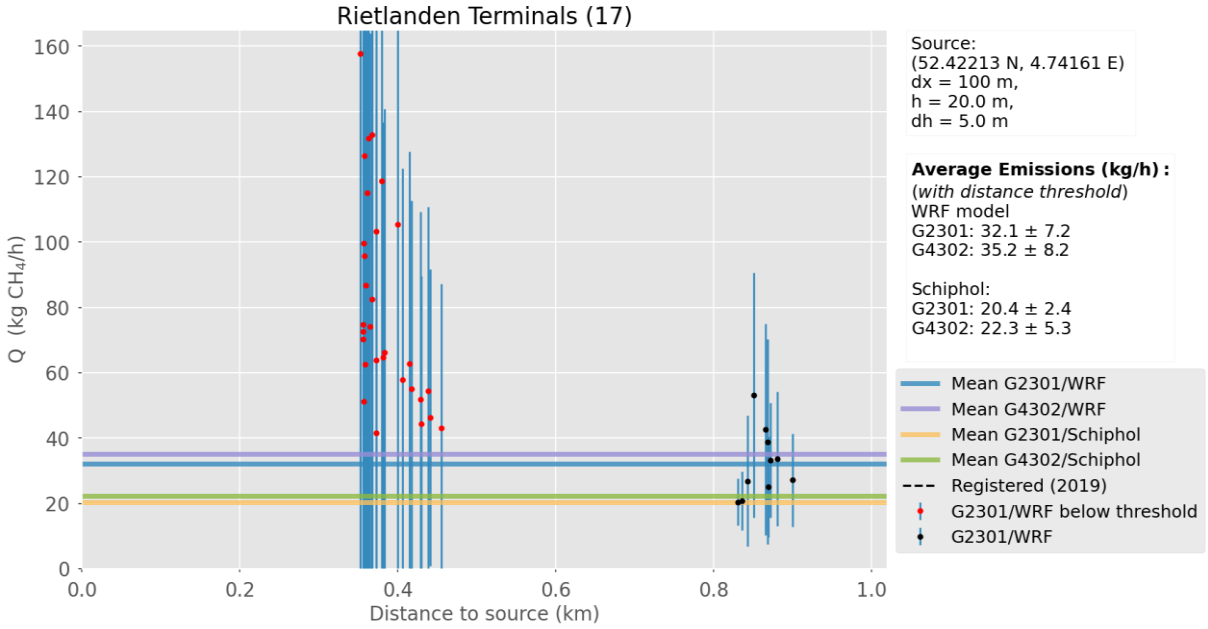

Figure 16. The G2301/WRF emission rates are shown at the difference from the source. It shows that the closest group of measurements, at 300 – 500 meters from the source, gives the highest rates with a maximum of 157.7 kg CH_4 h^{-1}. The average values range between 20.4 ± 2.4 kg CH_4 h^{-1} (G2301/Schiphol) and 35.2 ± 8.2 kg CH_4 h^{-1} (G4302/WRF), clearly distinguishing between the Picarro instruments and the meteorological methods.

4.2.9 Location 18: Vosse Groen Recycling (Waste)

Figure 17 shows the measurements at a downwind distance from Vosse Groen Recycling, with the emission rates using the G2301/WRF method. There are two groups of measurements, of which one below 100 meters distance, and one over 500 meters distance. The distance threshold is defined as 250 meters and excludes the first group of measurements.

The first group ranges between 36.8 ± 55.4 CH_4 h^{-1} and 93.7 ± 143.2 kg CH_4 h^{-1} at 81/82 meters distance. The second group ranges between 6.4 ± 2.2 kg CH_4 h^{-1} at 544 meters distance and 22.9 ± 13.9 kg CH_4 h^{-1} at 639 meters distance. The G4302/WRF method shows the highest average, at 18.7 ± 2.8 kg CH_4 h^{-1}. The G2301/WRF method averages at 16.0 ± 3.0 kg CH_4 h^{-1} and the Schiphol method gives averages of 14.1 ± 1.4 kg CH_4 h^{-1} (G2301) and 16.3 ± 1.9 kg CH_4 h^{-1} (G4302). This facility had no methane emissions registered.

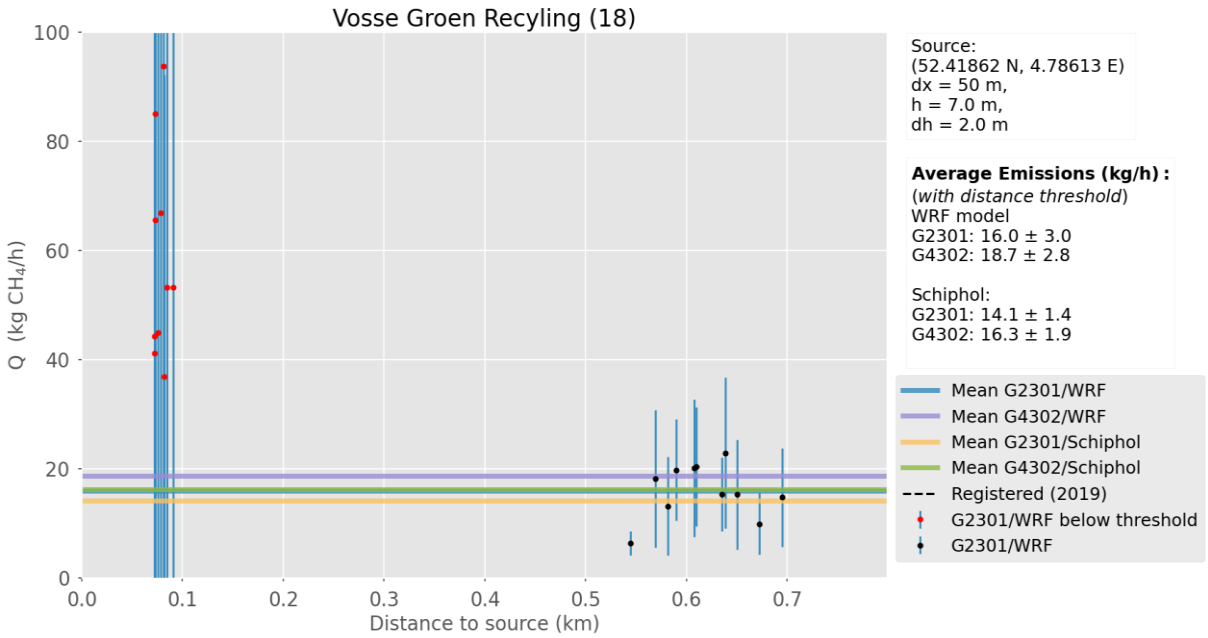

Figure 17. The G2301/WRF emission rates for Vosse Groen Recycling. The figures show two sets of measurements, one below 100 meters distance and one around 600 meters. The closer group ranges between 36.8 ± 55.4 CH_4 h^{-1} and 93.7 ± 143.2 kg CH_4 h^{-1} but is excluded by the distance threshold. Therefore, the averages are calculated with the second group only, which gives averages between 14.1 pm 1.4 kg CH_4 h^{-1} (G2301/Schiphol method) and 18.7 pm 2.8 kg CH_4 h^{-1} (G4302/WRF method).

4.2.10 Locations without quantification

At 6 locations, no methane enhancements were observed, but with limited or no access close to the facility. At 4 locations, clear methane enhancements were observed close to the facility, without the possibility of measuring transects. The locations are described in Table 6.

Table 6. The locations without quantification. The left side shows facilities where no methane enhancements were observed but with only limited or no access to the surrounding area. The right column shows four facilities where clear methane emissions could be attributed to this facility but where the road structure did not allow transects.

NO DETECTION	EMISSIONS DETECTED
Location 5: Nuon Hemweg	Location 4: Bunge Netherlands
Location 9: Sonneborn Refined Products	Location 6: Cargill
Location 10: Main BV	Location 7: AEB
Location 11: Cabot Norit Nederland	Location 8: ICL Fertilizers Europe
Location 12: Oxea Nederland	
Location 16: Paro Amsterdam	

4.3 Overview of all locations

Figure 18 shows the locations with quantified emissions, with the averages of the four methods given as vertical bars with an uncertainty range. The locations with a registered emission rate (the WWTP) show a dashed bar with the rate. The other locations didn't have an expected emission rate. The red/green colour

of the facility name indicates the implementation of a distance threshold. This was the case at 7 of 9 locations and always led to decreased emission rate averages.

Based on the quantification, Landfill Nauerna is the most emitting methane source in the Amsterdam harbour region. The highest officially registered source, WWTP Amsterdam-West, is only the 5th largest methane source, after the OBA and Rietlanden Terminals and Dutch Cacao.

Individual facility results show a pattern of higher emissions at close distances, stabilising to a more constant emission rate at larger distances. All emissions below a certain distance to the source were excluded by the distance threshold of *5 dx*, to find this stable emission rate. Implementation of this threshold was not possible at WWTP Amsterdam-West and WWTP Zaandam-Oost, where it would exclude all measurements. The averages for those facilities were calculated without the threshold.

At 6 out of 9 locations, the combination of the Picarro G4302 together with the WRF meteorological data gave the highest average emission rate. At 2 locations, the G2301/WRF combination gave the highest average, and at one location, it was the G2301/Schiphol combination.

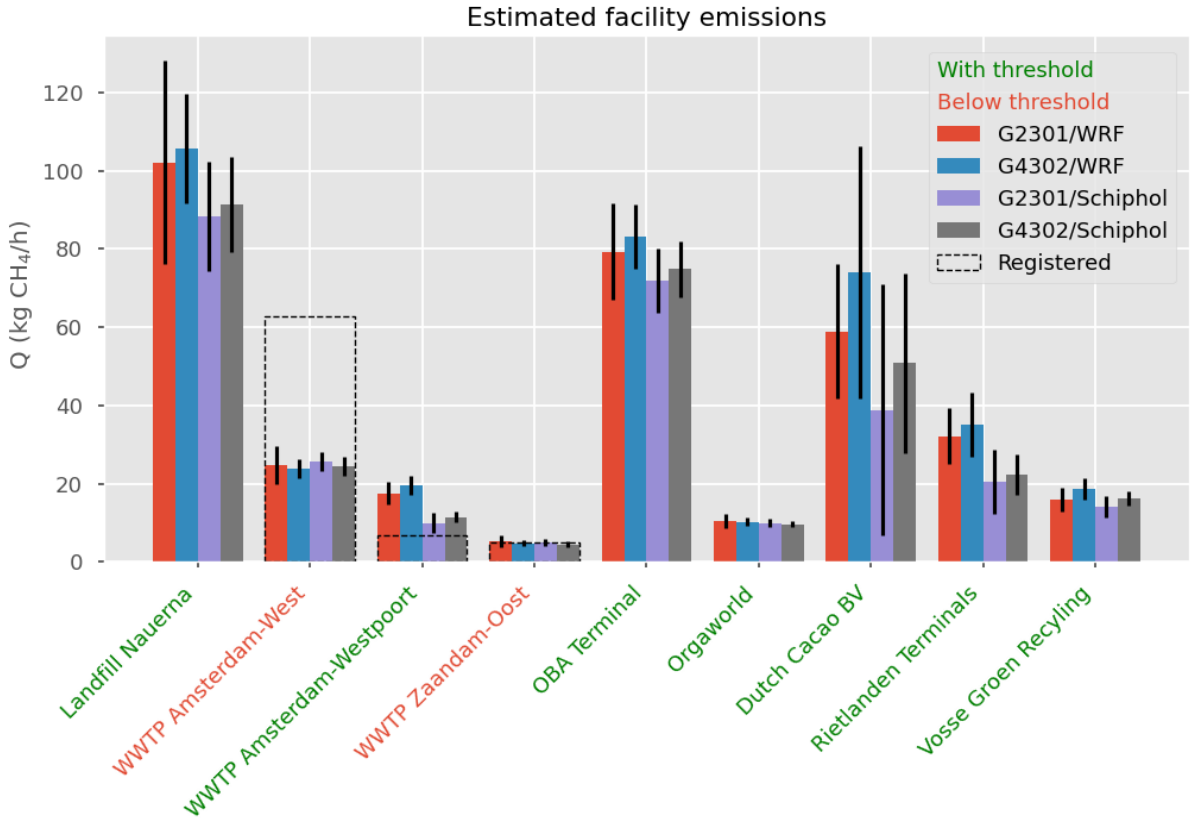

Figure 18. Overview of all quantified locations. For each facility, the vertical bars show the average emission rate for each of the four methods. The dashed vertical bar shows the expected emission rate based on an earlier measurement campaign for Landfill Nauerna and the registered emissions for the three WWTPs. The last five facilities had no emissions registered. The colour of the facility name indicates whether the averages for the facility are calculated with measurements that passed the distance threshold. The figure shows that the first two facilities, for which the highest emissions were expected, emit roughly half of the expected amounts. The 5 facilities without expected emissions all emit more than the smallest WWTP. Compared to WWTP Amsterdam-West, the highest registered facility, the two coal transhipment terminals are quantified at similar or larger emission rates.

4.4 Methodological comparison

4.4.1 Horizontal dispersion parameter

In the analysis, the cross-wind horizontal dispersion parameter σ_y is based on the width of the Gaussian shape fitted to the measured plume. The theoretical σ_y can also be calculated with the stability class and the distance to the source (as described in 3.4.2.2). Figure 19 shows that this alternative method gives roughly two times lower emission rates for all locations, except for Dutch Cacao, of which the G4301 emission rates increased.

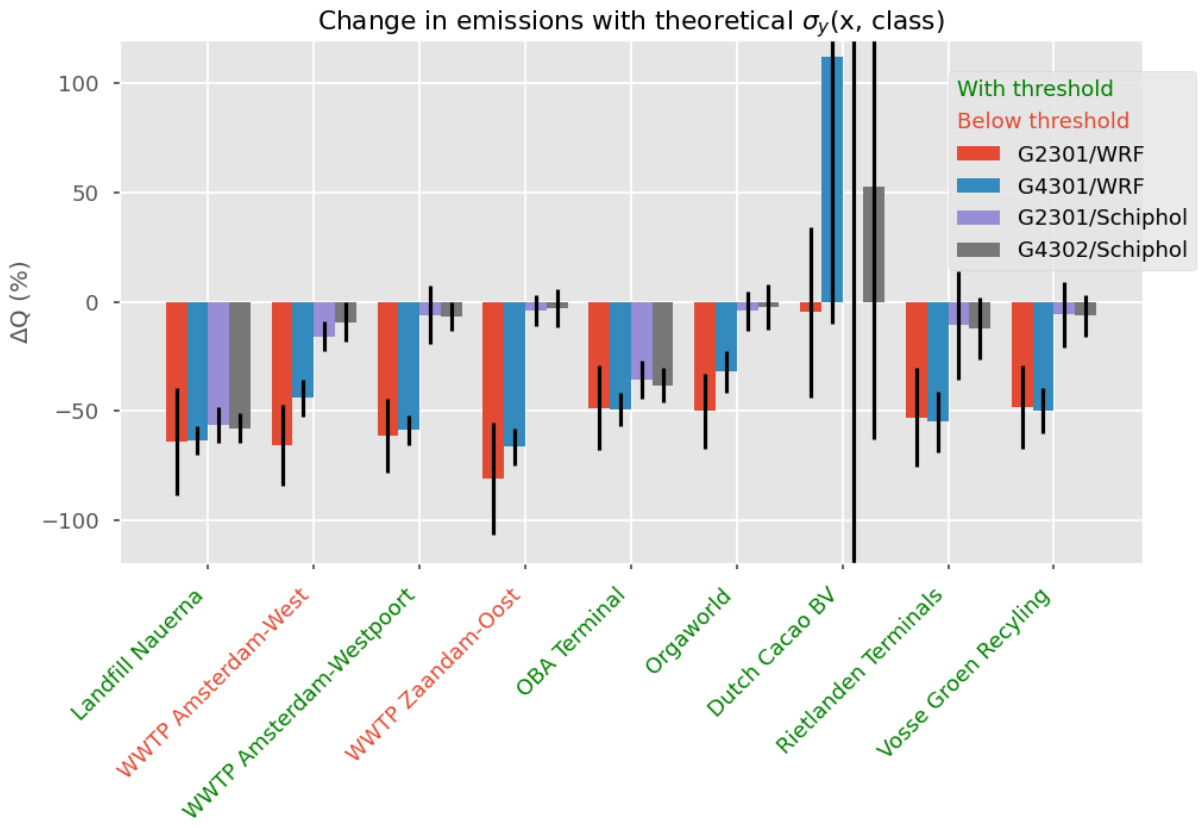

Figure 19. This overview shows the change in the quantified emission rates at all locations when an alternative method for choosing the cross-wind horizontal dispersion parameter σ_y is used. This method calculates the σ_y based on the distance from the source (x) and two parameters, c and d, based on the stability class. The standard method retrieves σ_y from fitting a Gaussian shape to the measured plume.

4.4.2 Meteorological datasets

Figure 20 compares the shortwave radiation retrieved from the WRF model and the KNMI Schiphol observations and the influence of the difference on emission rates. The bottom-left panel shows that the Schiphol dataset has larger shortwave radiation, with a fitted linear relation of 0.634. The difference in short-wave radiation only influences the quantification when it leads to a difference in stability class. The upper panel shows that this was the case for one day only. On 15/03/2022, the Schiphol data gave a stability class C, whereas the WRF model data gave stability class D. The bottom-right panel shows the difference between the results for both methods, but only for the transects on this day (15/03), with a difference in stability class. It shows two groups of emission rates, from two different facilities, with a fitted linear relation of 2.85 between the shown quantified emissions for both methods.

Figure 21 shows the relation between the windspeeds for both datasets and their influence on the quantification. The left panel shows the relation between the windspeeds for all transects. The amount of transects visible is limited, as most sets of transects used the same hourly averaged wind speed value. The relation between both data sets shows a fitted linear regression line with a slope of 1.24, indicating 1.2 times stronger wind speeds for the WRF model. The right panel shows the influence of this difference on the quantification. It shows a clear correlation, with the largest difference in wind speed (-75%) showing the exponential difference in emission rates (up to -160%), but the other data points show a more linear relation.

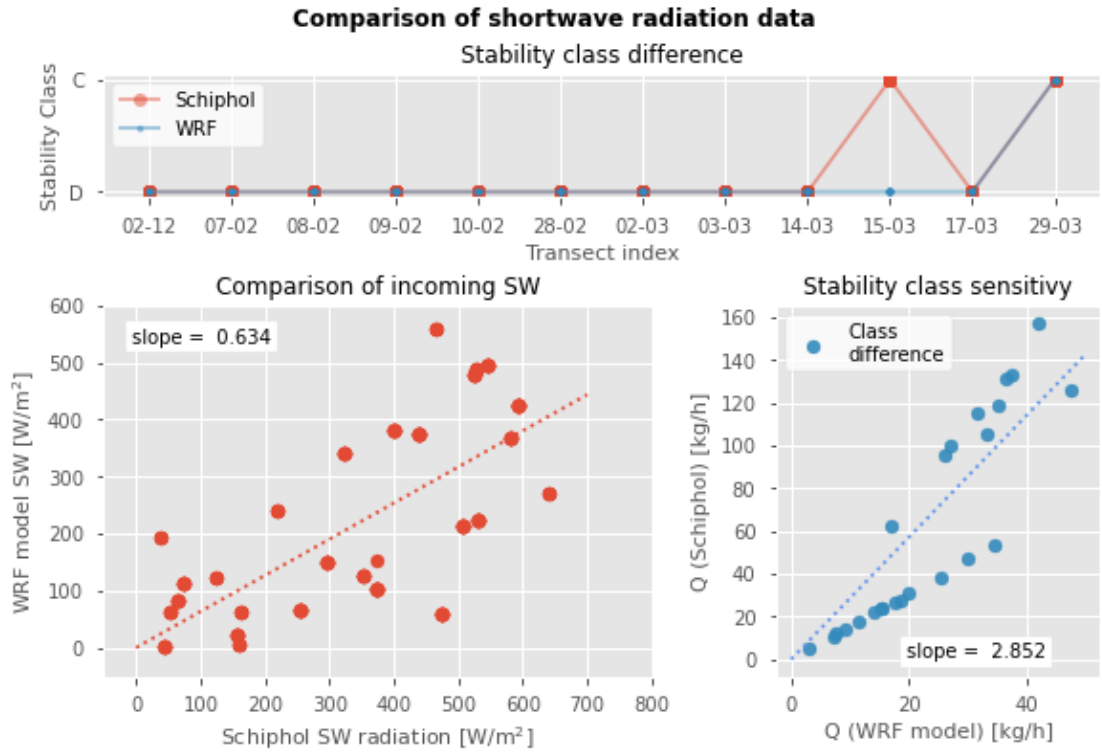

Figure 20. The comparison of shortwave radiation data from the WRF model and Schiphol meteorological datasets. The upper panel gives the stability class based on the two different datasets and shows that they differ only on 15-03. The bottom left panel scatters the SW radiation for both datasets and shows the regression line with a slope of 0.634. The bottom right panel shows emission rates for the transects only at which the stability class differed (15-03). A linear regression line was fitted for the data shown, showing that the Schiphol results (with stability class C) are 2.85 times larger on this day.

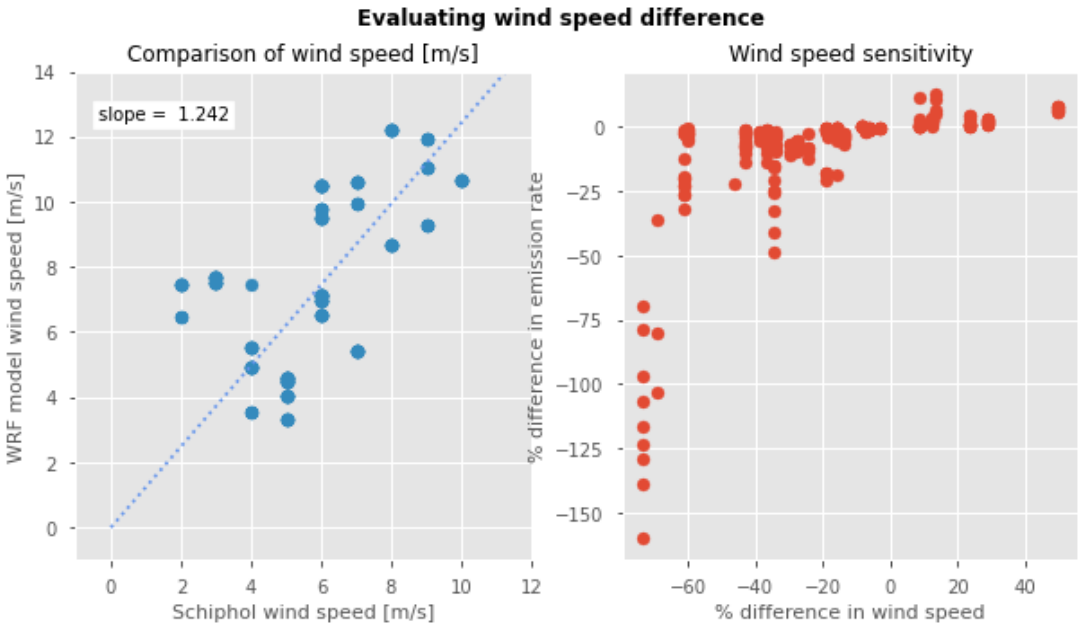

Figure 21. The left figure compares the wind speed during the transects for the WRF model and Schiphol meteorological datasets. A fitted linear regression line shows a slope of 1.2, indicating the general relation between the wind speeds from both sources. The right figure shows the influence that this wind speed difference between both datasets has on the quantified emission rates based on the Schiphol data (compared to WRF) plotted against the difference in wind speed.

5 Discussion

5.1 Detection

5.1.1 Availability and choice of roads

Twelve facilities with methane emissions were detected in the Port of Amsterdam area, but there might have been more methane-emitting facilities that have stayed unnoticed. The more extensive facilities,

such as chemical/fossil storage tank facilities, were often so large that all roads in/around the area were private property. This, combined with a large number of waterways, made it often impossible to measure close enough. Other techniques, such as measurements by UAVs or boats, could identify new sources of methane emissions in inaccessible parts of the port.

The project assumed constant emissions at all facilities throughout the day. The time of measuring could have influenced the quantification results in two different ways. Working hours might influence methane emissions for a processing plant such as Dutch Cacao. Our measurements were often during local working hours, but they sometimes went on until 19:00. This might have influenced methane detection. Furthermore, methane emissions can fluctuate throughout the year. With knowledge about this fluctuation, the emissions could be corrected to calculate yearly emission estimates.

Comparing the pattern of emission rates over distance at the different locations, closer measurements often led to emission rates of multiple factors above the average. As the distance got larger, the emission rates seemed to be stabilising. Measurements at a larger distance are more reliable in the GPDM because it assumes emissions coming from a point source.

The distance at which the measurements were stabilised always agreed with the distance of 5 times the uncertainty in source location *dx*. This threshold was chosen as it was consistent and because *dx* often reflected the size of the source area. A larger source area of emissions would need measurements at a larger distance. This relation between uncertainty and threshold is not correct when the emissions actually come from a point source. When the source location can be more accurately determined, *dx* would go down. But a better-attributed source location doesn't lead to other plume behaviour. So in this case, the threshold shouldn't get lower. Therefore, this threshold should not necessarily be recommended to other researchers. But in this research, the threshold successfully determines the distance after which the emissions have stabilised. Therefore, after implementing the threshold, the results can be seen as the more reliable emission rates.

5.1.2 Measurements and instruments

The GPS mobile device showed flaws at some points (such as recording 50 meters below mean sea level). When such apparent flaws were noticed, the backup recordings were used, which raised questions about the reliability of the other recordings. But as the quantification method relies strongly on the distance from the source, an offset of a few meters can already have consequences. Therefore, a more precise GPS recorder could be used in a successive campaign.

The Picarro instruments could have been calibrated more often to UTC to improve preciseness in the measurements. The UTC/delay time correction was based on measurements at the beginning of the day, but the data often needed extra corrections to overlap both instruments' methane peaks. This is sufficient for agreement between the Picarro instruments, but the agreement with the GPS times could, at this point, not be verified anymore. Establishing a constant internet connection at both Picarro instruments might be an easy solution.

Lastly, the driving speed varies between 25-60 km/h for the different locations. The influence of the driving speed on the measurements is unknown and might be assessed in further research.

5.2 Meteorological data

The public accessible meteorological data in the Port of Amsterdam was limited. Deploying a mobile weather station while transects were conducted would have improved the research method.

Therefore, the WRF model and KNMI Schiphol hourly average datasets were used. Using the wind directions from those datasets to attribute peaks to a source location showed the inaccuracy, as wind directions sometimes pointed 180 degrees towards the wrong location and showed no overlap for different measurement days. This was solved by assuming the wind direction to be from the assumed source location to the peak location. The wind speeds were still used from the hourly average datasets, as hourly averaged meteorological data is also recommended by Bailey (2000).

Furthermore, a method to correct the wind speed for the source height might improve results. For most locations, the source height was too uncertain, or the source could be assumed within the surface roughness layer. But in the case of a high chimney, as at Dutch Cacao, the wind speed could be corrected using a wind profile.

The WRF model uses the meteorological observations of multiple weather stations. It can be usefully applied to areas without a closely located weather station, such as the Port of Amsterdam. Towards the end of this project, the WRF model became inaccessible as nudging errors were established in the model. Therefore, the model data was not used for the last day of measurements. But more importantly, it raises questions about the reliability of the data.

Compared with Schiphol's observations, the WRF wind speeds tend to be 1.2 times larger. The WRF model is divided into 20 vertical layers. Therefore, the average of the bottom layer does not agree with the 2-meter wind speed. Further research could correct for this height when assuming a 2-meter windspeed.

There is no apparent cause for the significant difference in SW radiation between both datasets. This could even be an example of the nudging error in the WRF model. Comparing KNMI data and the WRF model at the coordinates of some KNMI stations could give more insight into this relation. But as the resulting stability class differed on one day only, the SW radiation difference influence on the results is limited.

The WRF model became inaccessible in May 2022 because calculation errors were found. The influence of these errors on the retrieved data, and thus the reliability of the WRF data to represent the actual conditions in the Port of Amsterdam, remains unknown.

The data of the private wind stations at Landfill Nauerna or Rietlanden Terminals could create insight into which of the meteorological methods is the most representative of the actual conditions.

5.3 Attribution

The mobile measurements' live data in the van proved to be a suitable method for attributing methane peaks to the sources. Measuring at different sides of the facility and with different wind directions convincingly showed where the enhanced plumes came from.

To use the GPDM, a single-point source was assumed and chosen for each location. Those choices were based on the observed peak locations at specific wind directions and expected source types. Communication with the facilities about the specific source location was unsuccessful but might help choose the best point source coordinates.

Furthermore, for Nauerna, Rietlanden and OBA Terminals, close measurements regularly identified multiple methane peaks. This indicates how information about the source locations would probably tell how the emissions are concentrated around a few locations on the site. Amplifying the GDPM to process multiple point sources could improve the accuracy of the results.

5.4 Quantification

5.4.1 Data processing and Gaussian fitting

The method of choosing a background value in a 10-minute rolling average was already different from the 5-minute rolling average in Maazallahi et al. (2020) but still shows small peaks in the background value during larger peaks. Choosing a fixed background value for each transect could be more accurate.

The Gaussian fitting method elegantly combined the measured plume's width and height into a gaussian shape and was used to provide the horizontal dispersion parameter, just as in Maazallahi et al. (2020). Calculating this parameter based on distance and stability class gives significantly different results (4.4.1), which shows the importance of this parameter very well.

Because of the low frequency of wind direction data, the vector between the location of the Gaussian peak and the assumed point source was taken as the wind direction. But due to turbulence, some outliers were often identified further down the road. As this increases the distance to the source, this could improve the

measurement. But often, this led to the wind direction being not perpendicular anymore. Further research could, in this case, correct the σ_y for this change in angle.

5.4.2 Quantification results

The four different methods led to four different emission rates per transect. There was no apparent reason to choose one outcome and no method to combine the four outcomes into a single version.

Figure 22 shows that at 6 out of 9 locations, the G4302/WRF method gave the largest average emission rate. At the other locations, it was twice the G2301/WRF and once the G2301/Schiphol method. This shows that the WRF model dataset method in almost all cases gave the largest emission rate results.

The G4301 and G2301 Picarro results were closer to each other than the meteorological results for the same Picarro. The G4301 often, but not always, gave the higher results.

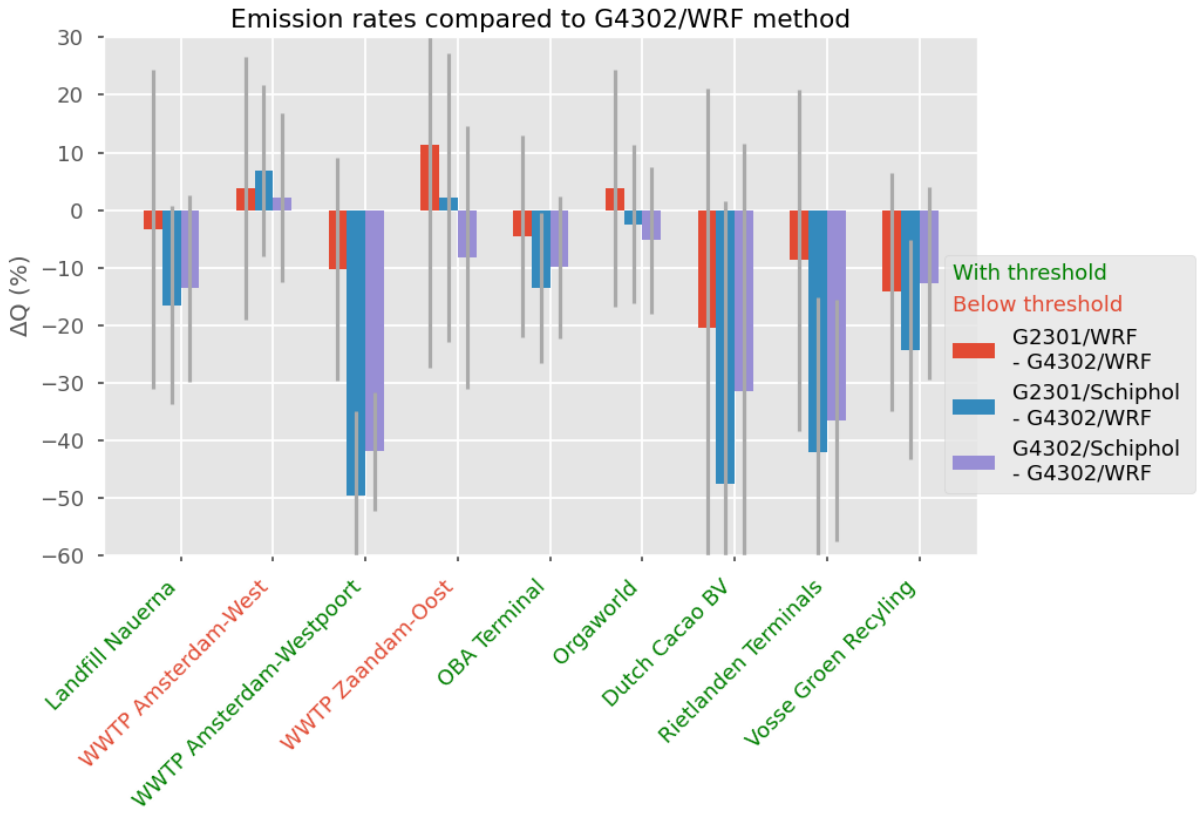

Figure 22. The different emission rates per method, compared to the G4302/WRF method, which in most cases led to the largest average emission rate.

The uncertainty on the final emission rates is calculated by simple error propagation but misses a logarithmic type of scaling on the negative side, as the uncertainty range sometime gets to/below zero emissions, which shouldn't be the case when the methane emissions are attributed to a facility with certainty.

But more importantly, variability and uncertainty are regarded as similar phenomena in this approach, which shouldn't be the case. The variability in measurements on a single day, most often within 30 minutes, can be deservedly regarded as uncertainty on the actual emissions at that moment. But at most locations, the measurements were spread out over different days, with possible variability in the actual emissions for each day. Further research could develop a method to exclude the day-to-day variability from the uncertainty calculation and find a correct way to present this variability.

5.5 Facilities

5.5.1 Facilities with registered emissions

The WWTP Amsterdam-West, the biggest of the three WWTs, surprisingly showed emission rates (around 25 kg CH_4 h^{-1}) that were not even half of the registered emissions (63 kg CH_4 h^{-1}). These measurements are

at a close distance, below the threshold, so they could even overestimate emission rates. There is no clear explanation for this difference compared to the registered emissions. The 25 kg CH_4 h^{-1} is in the same order of magnitude as the observations at WWTP Utrecht by Maazallahi et al. (2020) (18 kg CH_4 h^{-1}), but in Utrecht, it matched the registered emissions quite well.

The emission rates at WWTP Amsterdam-Westpoort are well above registered emissions and not much below the WWTP Amsterdam-West emissions. A large difference was expected as the sludge treatment for both locations happens in WWTP Amsterdam-West, which also has a significantly larger capacity.

The third WWTP in Zaandam, which has the least clear connection to the Port of Amsterdam, shows emission rates that match the registered emissions very well. But with only one measurement day, of which all measurements did not pass the distance threshold, the uncertainty in the emission rate might be underestimated.

Of all registered facilities, these three WWTPs were the most important, as the sum of their registered emissions is over 95% of all registered emissions. The measured value for Amsterdam-West is the only one below the registered amount but is only based on two days of measurements on a closely located road. More measurements should verify this decrease from the 2019 registered emissions throughout the year.

5.5.2 Facilities without registered emissions

The six other locations that were quantified all had no registered methane emissions, whereas 4 out of 6 showed higher emissions than WWTP Amsterdam West, which was the highest registered emitter.

It is unclear why Landfill Nauerna had no registered methane emissions in the national inventory. All other landfills by Afvalzorg did have registered methane emissions, and this location has registered other emissions. Furthermore, Landfill Nauerna's methane emissions are monitored multiple times, with its most recent campaign estimating 171.2 kg CH_4 h^{-1}. The results at Landfill Nauerna were a primary example of the need for the distance threshold, as the emissions on the two closer roads were significantly higher than the emissions at the furthest road. When the distance threshold was implemented, the highest emission rate average was 105.7 ± 14 kg CH_4 h^{-1} kg CH_4 h^{-1} (G4302/WRF), which is well below the expected emissions rate of 171.2 kg CH_4 h^{-1}.

For all other locations, no earlier emission estimates are known. Of those five, the OBA Terminal showed the highest emission estimates, with a maximum of 83.1 ± 8.2 kg CH_4 h^{-1} (G4302/WRF). The excluded measurements at the closest roads are higher, but the two remaining sets of measurements, around 500 and 1300 meters, agree well. The furthest measurements were across a waterway and a large vehicle storage park, showing how successful measurements can still be done with multiple objects in between.

Orgaworld, a waste processor and biogas producer, showed significant variability, with two outliers strongly increasing the average results after applying the threshold. It stands out how the average results for the four different methods agree very well, within the uncertainty range of the largest average of 10.6 ± 1.8 kg CH_4 h^{-1} (G2301/WRF).

The average results for Dutch Cacao diverge a lot, showing considerable uncertainty for all methods. The source of this location was assumed to be on top of the chimney, at 38 meters. This was supported by the fact that the measurements directly next to the facility did not show any enhancements, whereas a road further away did show enhancements. But the measurements at the further road showed enhancements at only 15/56 transects. Due to the large height of the chimney, measurements of a minor methane enhancement immediately lead to large emission rates in the GPDM. But given the fact that transects without a usable methane signal are not represented in the average values, the methane emissions for this facility are probably overestimated. Furthermore, the emission estimates with a theoretical σ_y lead to incoherent changes at this location. The change is different per method and clearly out of line compared to the changes at the other facilities.

The Rietlanden Terminals could also be measured at a distance across a waterway, showing a significant decrease in emission rates over the distance again. The WRF method emission rates are 50% larger than the Schiphol emission rates, showing the influence of the method.

Lastly, Vosse Groen Recycling shows a significant difference between the closer and further measurements, with the first set below 100 meters to the source. Quantification with the threshold gives results between 14.1 ± 1.4 – 18.7 ± 2.8 kg CH_4 h^{-1}, similar to WWT-Westpoorts emissions.

5.5.3 Facilities without quantification

Facilities 11 (Cabot Norit) and 16 (Paro Amsterdam) were not visited. Paro could still be visited for transects with northern wind, and Cabot Norit could be visited with the wind from the east. Measurements by boat, or access to private property, would be necessary to measure the other non-quantified facilities.

6 Conclusions

The results show that mobile measurements can be used to cross-check emission reports and identify unreported locations. Of 12 facilities with registered emissions in the Amsterdam harbour area, CH_4 emissions were successfully quantified at 3 facilities. These 3 WWTPs, account for over 95% of all registered emissions. The average emission rate estimates at WWTP Amsterdam West are roughly half of their registered emissions. Furthermore, similar emission rates were found at WWTP Amsterdam-Westpoort, which was registered at a 10 times lower emission rate. The other facilities with registered emissions could not be quantified, but as they make up roughly 4% of the total registered amount of emissions, most of them emit very low rates that are hard to measure with the GPDM method.

Surprisingly, most of the quantified emissions were found at non-registered facilities. The CH_4 emissions from Landfill Nauerna and two coal transhipment facilities should not surprise the registration authorities, as the landfill has been registered multiple times over the last decades, and fossil fuels are one of the most important anthropogenic emitters of methane. Also, a cacao processing plant, a biogas producer and an organic waste collector were quantified at emission rates larger than WWTP Zaandam, the third-largest registered emitter. As many canals and a lack of public roads prohibited measurements around multiple facilities, it can not be excluded that some emitters are overlooked. Further measurements are needed to verify the findings, and measurements by boat or UAV could be used to quantify the remaining facilities.

7 References

Abdel-Rahman, A. A. (2011). On the dispersion models and atmospheric dispersion. *International Journal of Global Warming*, *3*(3), 257-273. https://doi.org/10.1504/ijgw.2011.043422

Afvalzorg. (2022). *Locatie Nauerna*. Retrieved 23-05-2022 from https://www.afvalzorg.nl/locaties/locatie-nauerna/

Alvarez, R. A., Zavala-Araiza, D., Lyon, D. R., Allen, D. T., Barkley, Z. R., Brandt, A. R., Davis, K. J., Herndon, S. C., Jacob, D. J., Karion, A., Kort, E. A., Lamb, B. K., Lauvaux, T., Maasakkers, J. D., Marchese, A. J., Omara, M., Pacala, S. W., Peischl, J., Robinson, A. L., . . . Hamburg, S. P. (2018). Assessment of methane emissions from the U.S. oil and gas supply chain. *Science*, *361*(6398), 186-188. https://doi.org/doi:10.1126/science.aar7204

Amsterdam, P. o. (2022). *Over Port of Amsterdam*. Port of Amsterdam. Retrieved 14-01-2022 from https://www.portofamsterdam.com/nl/over-port-amsterdam

Andersen, T., De Vries, M., Necki, J., Swolkien, J., Menoud, M., Röckmann, T., Roiger, A., Fix, A., Peters, W., & Chen, H. (2022). *Local to regional methane emissions from the Upper Silesia Coal Basin (USCB) quantified using UAV-based atmospheric measurements*. Copernicus GmbH. https://dx.doi.org/10.5194/acp-2021-1061

Armstrong, J. (2022). *EU Ports' Climate Performance. An analysis of maritime supply chain and at berth emissions*. https://www.transportenvironment.org/discover/port-carbon-emissions-ranking/

Bailey, D. T. (2000). *Meteorological Monitoring Guidance for Regulatory Modeling Applications* (EPA-454/R-99-005).

Chen, J., Dietrich, F., Maazallahi, H., Forstmaier, A., Winkler, D., Hofmann, M. E. G., Denier Van Der Gon, H., & Röckmann, T. (2020). Methane emissions from the Munich Oktoberfest. *Atmospheric Chemistry and Physics*, *20*(6), 3683-3696. https://doi.org/10.5194/acp-20-3683-2020

Cui, Y. Y., Brioude, J., McKeen, S. A., Angevine, W. M., Kim, S.-W., Frost, G. J., Ahmadov, R., Peischl, J., Bousserez, N., Liu, Z., Ryerson, T. B., Wofsy, S. C., Santoni, G. W., Kort, E. A., Fischer, M. L., & Trainer, M. (2015). Top-down estimate of methane emissions in California using a mesoscale inverse modeling technique: The South Coast Air Basin. *Journal of Geophysical Research: Atmospheres*, *120*(13), 6698-6711. https://doi.org/10.1002/2014jd023002

Dlugokencky, E. (2021, 05/01/2022). *NOAA/GML*. gml.noaa.gov/ccgg/trends_ch4/

Dlugokencky, E. J., Steele, L. P., Lang, P. M., & Masarie, K. A. (1994). The growth rate and distribution of atmospheric methane. *Journal of Geophysical Research: Atmospheres*, *99*(D8), 17021-17043.

Etminan, M., Myhre, G., Highwood, E., & Shine, K. (2016). Radiative forcing of carbon dioxide, methane, and nitrous oxide: A significant revision of the methane radiative forcing. *Geophysical Research Letters*, *43*(24), 12,614-612,623.

Fernández-González, S., Martín, M. L., García-Ortega, E., Merino, A., Lorenzana, J., Sánchez, J. L., Valero, F., & Rodrigo, J. S. (2018). Sensitivity Analysis of the WRF Model: Wind-Resource Assessment for Complex Terrain. *Journal of Applied Meteorology and Climatology*, *57*(3), 733-753. https://doi.org/10.1175/jamc-d-17-0121.1

Fiehn, A., Kostinek, J., Eckl, M., Klausner, T., Gałkowski, M., Chen, J., Gerbig, C., Röckmann, T., Maazallahi, H., & Schmidt, M. (2020). Estimating CH 4, CO 2 and CO emissions from coal mining and industrial activities in the Upper Silesian Coal Basin using an aircraft-based mass balance approach. *Atmospheric Chemistry and Physics*, *20*(21), 12675-12695.

Gålfalk, M., Nilsson Påledal, S., & Bastviken, D. (2021). Sensitive Drone Mapping of Methane Emissions without the Need for Supplementary Ground-Based Measurements. *ACS Earth and Space Chemistry*, *5*(10), 2668-2676. https://doi.org/10.1021/acsearthspacechem.1c00106

Helfter, C., Tremper, A. H., Halios, C. H., Kotthaus, S., Bjorkegren, A., Grimmond, C. S. B., Barlow, J. F., & Nemitz, E. (2016). Spatial and temporal variability of urban fluxes of methane, carbon monoxide and carbon dioxide above London, UK. *Atmospheric Chemistry and Physics*, *16*(16), 10543-10557. https://doi.org/10.5194/acp-16-10543-2016

Hensen, A., Erisman, J., Fossiel, E.-S., Cnubben, P., & van der Klein, C. (2000). *Op zoek naar onbekende bronnen van broeikasgassen*. Energieonderzoek Centrum Nederland.

Hensen, A., Slanina, J., & van der Klein, C. A. M. (2000). *Methaanemissie van de deponie Nauerna: november 1999*. Petten: ECN.

Jacobs, J., Scharff, H., Hensen, A., Kraai, A., Scheutz, C., & Samuelsson, J. (2007). Testing a simple and low cost methane emission measurement method. Proceedings Sardinia,

Karion, A., Sweeney, C., Pétron, G., Frost, G., Michael Hardesty, R., Kofler, J., Miller, B. R., Newberger, T., Wolter, S., Banta, R., Brewer, A., Dlugokencky, E., Lang, P., Montzka, S. A., Schnell, R., Tans, P., Trainer, M., Zamora, R., & Conley, S. (2013). Methane emissions estimate from airborne measurements over a western United States natural gas field. *Geophysical Research Letters*, *40*(16), 4393-4397. https://doi.org/10.1002/grl.50811

Kort, E. A., Eluszkiewicz, J., Stephens, B. B., Miller, J. B., Gerbig, C., Nehrkorn, T., Daube, B. C., Kaplan, J. O., Houweling, S., & Wofsy, S. C. (2008). Emissions of CH4and N2O over the United States and Canada based on a receptor-oriented modeling framework and COBRA-NA atmospheric observations. *Geophysical Research Letters*, *35*(18). https://doi.org/10.1029/2008gl034031

Lushi, E., & Stockie, J. M. (2010). An inverse Gaussian plume approach for estimating atmospheric pollutant emissions from multiple point sources. *Atmospheric Environment*, *44*(8), 1097-1107. https://doi.org/10.1016/j.atmosenv.2009.11.039

Maazallahi, H., Fernandez, J. M., Menoud, M., Zavala-Araiza, D., Weller, Z. D., Schwietzke, S., von Fischer, J. C., Denier van der Gon, H., & Röckmann, T. (2020). Methane mapping, emission quantification, and attribution in two European cities: Utrecht (NL) and Hamburg (DE). *Atmospheric Chemistry and Physics*, *20*(23), 14717-14740.

McKain, K., Down, A., Raciti, S. M., Budney, J., Hutyra, L. R., Floerchinger, C., Herndon, S. C., Nehrkorn, T., Zahniser, M. S., Jackson, R. B., Phillips, N., & Wofsy, S. C. (2015). Methane emissions from natural

gas infrastructure and use in the urban region of Boston, Massachusetts. *Proceedings of the National Academy of Sciences*, *112*(7), 1941-1946. https://doi.org/10.1073/pnas.1416261112

Morales, R., Ravelid, J., Vinkovic, K., Korbeń, P., Tuzson, B., Emmenegger, L., Chen, H., Schmidt, M., Humbel, S., & Brunner, D. (2021). A tracer release experiment to investigate uncertainties in drone-based emission quantification for methane point sources [under review]. *Meas. Tech. Discuss. [preprint]*. https://doi.org/10.5194/amt-2021-314

Myhre, G., Shindell, D., Bréon, F., Collins, W., Fuglestvedt, J., & Huang, J. (2013). Anthropogenic and Natural Radiative Forcing In: Stocker TF, Qin D, Plattner GK, Tignor M, Allen SK, Boschung J, et al., editors. Climate change 2013: The physical science basis Contribution of working group 1 to the fifth assessment report of the intergovernmental panel on climate change. Cambridge, United Kingdom and New York, NY. In: USA: Cambridge University Press.

Nisbet, E. G., Manning, M. R., Dlugokencky, E. J., Fisher, R. E., Lowry, D., Michel, S. E., Myhre, C. L., Platt, S. M., Allen, G., Bousquet, P., Brownlow, R., Cain, M., France, J. L., Hermansen, O., Hossaini, R., Jones, A. E., Levin, I., Manning, A. C., Myhre, G., . . . White, J. W. C. (2019). Very Strong Atmospheric Methane Growth in the 4 Years 2014–2017: Implications for the Paris Agreement. *Global Biogeochemical Cycles*, *33*(3), 318-342. https://doi.org/https://doi.org/10.1029/2018GB006009

O'Shea, S. J., Allen, G., Fleming, Z. L., Bauguitte, S. J.-B., Percival, C. J., Gallagher, M. W., Lee, J., Helfter, C., & Nemitz, E. (2014). Area fluxes of carbon dioxide, methane, and carbon monoxide derived from airborne measurements around Greater London: A case study during summer 2012. *Journal of Geophysical Research: Atmospheres*, *119*(8), 4940-4952. https://doi.org/https://doi.org/10.1002/2013JD021269

Ocko, I. B., Naik, V., & Paynter, D. (2018). Rapid and reliable assessment of methane impacts on climate. *Atmospheric Chemistry and Physics*, *18*(21), 15555-15568. https://doi.org/10.5194/acp-18-15555-2018

Ocko, I. B., Sun, T., Shindell, D., Oppenheimer, M., Hristov, A. N., Pacala, S. W., Mauzerall, D. L., Xu, Y., & Hamburg, S. P. (2021). Acting rapidly to deploy readily available methane mitigation measures by sector can immediately slow global warming. *Environmental Research Letters*, *16*(5), 054042. https://doi.org/10.1088/1748-9326/abf9c8

Paredes, M. G., Güereca, L. P., Molina, L. T., & Noyola, A. (2019). Methane emissions from anaerobic sludge digesters in Mexico: On-site determination vs. IPCC Tier 1 method. *Science of The Total Environment*, *656*, 468-474. https://doi.org/https://doi.org/10.1016/j.scitotenv.2018.11.373

RIVM. (2022). *Emissieregistratie*. emissieregistratie.nl

Ruyssenaars, P., Coenen, P., Rienstra, J., Zijlema, P., Arets, E., Baas, K., Dröge, R., Geilenkirchen, G., t Hoen, M., & Honig, E. (2021). Greenhouse gas emissions in the Netherlands 1990–2019.

Ryoo, J.-M., Iraci, L. T., Tanaka, T., Marrero, J. E., Yates, E. L., Fung, I., Michalak, A. M., Tadić, J., Gore, W., Bui, T. P., Dean-Day, J. M., & Chang, C. S. (2019). Quantification of CO_2 and CH_4 emissions over Sacramento, California, based on divergence theorem using aircraft measurements. *Atmospheric Measurement Techniques*, *12*(5), 2949-2966. https://doi.org/10.5194/amt-12-2949-2019

Sadavarte, P., Pandey, S., Maasakkers, J. D., Lorente, A., Borsdorff, T., Denier van der Gon, H., Houweling, S., & Aben, I. (2021). Methane Emissions from Superemitting Coal Mines in Australia Quantified Using TROPOMI Satellite Observations. *Environmental Science & Technology*, *55*(24), 16573-16580. https://doi.org/10.1021/acs.est.1c03976

Saunois, M., Stavert, A. R., Poulter, B., Bousquet, P., Canadell, J. G., Jackson, R. B., Raymond, P. A., Dlugokencky, E. J., Houweling, S., Patra, P. K., Ciais, P., Arora, V. K., Bastviken, D., Bergamaschi, P., Blake, D. R., Brailsford, G., Bruhwiler, L., Carlson, K. M., Carrol, M., . . . Zhuang, Q. (2020). The Global Methane Budget 2000–2017. *Earth System Science Data*, *12*(3), 1561-1623. https://doi.org/10.5194/essd-12-1561-2020

Scharff, H., Martha, A., Van Rijn, D., Hensen, A., Flechard, C., Oonk, H., Vroon, R., de Visscher, A., & Boeckx, P. (2003). A comparison of measurement methods to determine landfill methane emissions. *Afvalzorg Deponie BV, Dutch ministry of Housing, spatial Planning and Environment*.

Skamarock, W. C., Klemp, J. B., Dudhia, J., Gill, D. O., Liu, Z., Berner, J., Wang, W., Powers, J. G., Duda, M. G., & Barker, D. M. (2019). A description of the advanced research WRF model version 4. *National Center for Atmospheric Research: Boulder, CO, USA*, *145*, 145.

Stocker, T. F., Qin, D., Plattner, G.-K., Alexander, L. V., Allen, S. K., Bindoff, N. L., Bréon, F.-M., Church, J. A., Cubasch, U., & Emori, S. (2013). Technical summary. In *Climate change 2013: the physical science*

basis. Contribution of Working Group I to the Fifth Assessment Report of the Intergovernmental Panel on Climate Change (pp. 33-115). Cambridge University Press.

Turnbull, J. C., Karion, A., Fischer, M. L., Faloona, I., Guilderson, T., Lehman, S. J., Miller, B. R., Miller, J. B., Montzka, S., Sherwood, T., Saripalli, S., Sweeney, C., & Tans, P. P. (2011). Assessment of fossil fuel carbon dioxide and other anthropogenic trace gas emissions from airborne measurements over Sacramento, California in spring 2009. *Atmospheric Chemistry and Physics*, *11*(2), 705-721. https://doi.org/10.5194/acp-11-705-2011

Turner, A. J., Frankenberg, C., & Kort, E. A. (2019). Interpreting contemporary trends in atmospheric methane. *Proceedings of the National Academy of Sciences*, *116*(8), 2805-2813. https://doi.org/10.1073/pnas.1814297116

Turner, D. B. (1994). *Workbook of atmospheric dispersion estimates: an introduction to dispersion modeling* (Second edition. ed.). Lewis Publishers.

Paris Agreement to the United Nations Framework Convention on Climate Change, (2015).

UNFCC. (2021). *World Leaders Kick Start Accelerated Climate Action at COP26* https://unfccc.int/news/world-leaders-kick-start-accelerated-climate-action-at-cop26

van Dinther, D., de Bie, S., Velzeboer, I., van den Bulk, P., Frumau, A., & Hensen, A. (2021). Defining sources from mobile gas measurements using their typical "fingerprint". EGU General Assembly Conference Abstracts,

van Nieuwenhuijzen, A. F., Havekes, M., Reitsma, B. A., & de Jong, P. (2009). Wastewater Treatment Plant Amsterdam West: New, Large, High-Tech and Sustainable. *Water Practice and Technology*, *4*(1). https://doi.org/10.2166/wpt.2009.006

Varon, D. J., Jacob, D. J., Jervis, D., & McKeever, J. (2020). Quantifying time-averaged methane emissions from individual coal mine vents with GHGSat-D satellite observations. *Environmental Science & Technology*, *54*(16), 10246-10253.

Walter, S., & Röckmann, T. (2019). MEMO2: MEthane goes MObile–MEasurements and MOdelling. *NCGG8*.

Yacovitch, T. I., Herndon, S. C., Pétron, G., Kofler, J., Lyon, D., Zahniser, M. S., & Kolb, C. E. (2015). Mobile Laboratory Observations of Methane Emissions in the Barnett Shale Region. *Environmental Science & Technology*, *49*(13), 7889-7895. https://doi.org/10.1021/es506352j

Yacovitch, T. I., Neininger, B., Herndon, S. C., van der Gon, H. D., Jonkers, S., Hulskotte, J., Roscioli, J. R., & Zavala-Araiza, D. (2018). Methane emissions in the Netherlands: The Groningen field. *Elementa: Science of the Anthropocene*, *6*. https://doi.org/10.1525/elementa.308

8 Appendices

8.1 Appendix 1: Description of individual facilities.

8.1.1 Location 0: Landfill Nauerna (Waste)

Figure 23 shows Landfill Nauerna, one of the multiple locations of the company Afvalzorg (Afvalzorg, 2022). It stores a large variety of soil/waste materials, focussing on building materials. From April 2022 onwards, it was closed because it had reached the maximum volume allowed. The top of the landfill was covered, and a recreational park was developed on top of a large part. This location has been the subject of multiple methane measurement campaigns, estimating 1.5 kton CH_4/y (Jacobs et al., 2007) to 3.4 kton CH_4/y (Hensen, Slanina, et al., 2000). This company does not come forward with registered emissions in the national inventory.

This location provides three possibilities for transects. The first is at the s150, directly to the south of the landfill. This road has the disadvantage of being close to the landfill and especially close to a small wastewater treatment situated next to the road. Also, this road is about 20 meters below the top of the landfill. The second possibility is on the east side of the landfill. This is a small road, sometimes resulting in a necessary stop in the middle of a transect to let oncoming traffic pass. The third and best option was at the N246, to the Northwest of the landfill. This location was preferred because the distance was the largest, reducing the influence of the height difference.

There were 4 days with transects downwind of Landfill Nauerna. At the s150, to the south of the Landfill, transects were measured on 02/12/21 and 29/03/22. The road to the northwest was measured on 14/03/22, and the N246 to the northwest was measured on 28/02/22.

Figure 23. Landfill Nauerna and the measurements at the public roads around it. The landfill is owned by Afvalzorg and was closed in April 2022 because it reached its maximum capacity. The yellow pointer indicates the assumed point source location.

8.1.2 Location 1: Wastewater Treatment Amsterdam West (WWTP)

WWTP Amsterdam West is the most prominent wastewater treatment location in the port. It covers the sewage and drinking water of the city's urban areas, with a capacity of 1.0 million population equivalents (p.e.). It is a modern complex, as it was completed in 2005, replacing two older WWTs in Amsterdam (van Nieuwenhuijzen et al., 2009). The sludge treatment also processes sludge from other WWTs. A direct pipeline transports liquid sludge from WWTP Westpoort (location 2), and thickened sludge is transported from other WWTs within the region of the regional water authority Amstel, Gooi en Vecht. Therefore, the

capacity of the sludge processing installation, which is the part of the process mainly responsible for methane emissions (Paredes et al., 2019), is even higher: 1.8 million p.e. The dewatered sludge is transported to the AEB (across the road to the north, see Figure 24), where it is incinerated in a high-efficient waste furnace (van Nieuwenhuijzen et al., 2009). The registered emissions in the national inventory are 549.5 tons CH_4/y (RIVM, 2022).

Public roads surround the WWT, but the traffic lights at the corners make the short sides unsuitable for transects. To the north of the WWT, the waste processing furnace (AEB) is located. This facility is also an emitter of methane, interfering with the WWTP emissions when the wind comes from the north. Therefore, only with southern wind, it was possible to do transects on the road to the north of the WWT.

Transects were measured at this road twice, on 28/02/22 and 15/03/22.

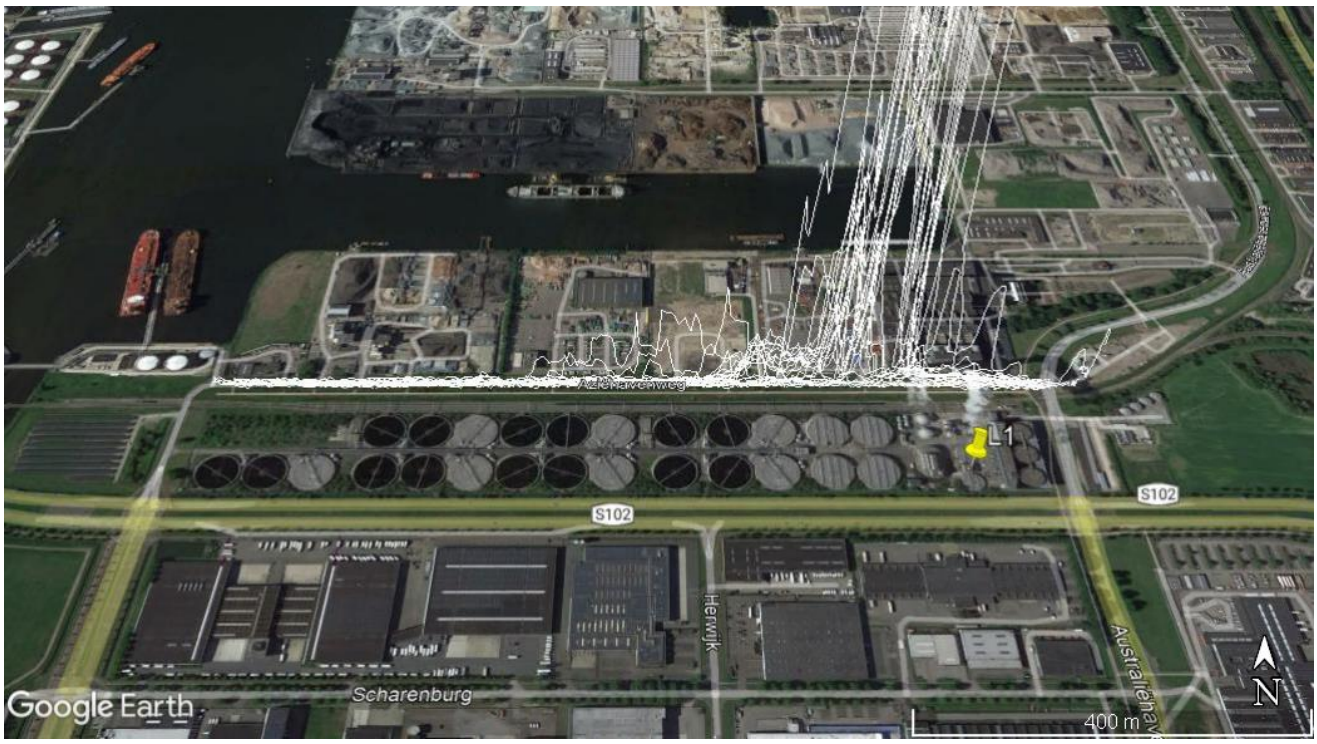

Figure 24. Wastewater Treatment Amsterdam West is the biggest WWTP in the Amsterdam region. It is surrounded by busy public roads with traffic lights and is situated to the south of AEB, the public waste processing plant of the municipality. This complicated the possibilities of doing transects. The yellow pointer indicates the assumed point source location.

8.1.3 Location 2: Wastewater Treatment Amsterdam Westpoort (WWTP)

WWTP Amsterdam Westpoort is situated in the proximity of WWTP Amsterdam West, but its capacity is more than two times smaller, at 400 000 p.e. (Koenders et al., 2011). The expected methane emissions are low as it can transport its liquid sludge to WWTP Amsterdam West. The registered methane emissions in the national inventory are ten times below the WWTP Amsterdam West emissions, at 59.6 tons CH_4/y (RIVM, 2022). There are public roads on the east, north and west side, but not all streets are perfectly perpendicular to the wind coming from the WWT. The best wind directions, therefore, are WNW-SW, SSE and NE.

Measurements were done on 07/02/22, 10/02/22, and 11/02/22. But during those days, a large NGDN leak located next to the WWTP was found and estimated to emit 160 L CH_4 min^{1}. Therefore, these days had to be discarded. On 14/03/22, 29/03/22 and 13/05/22, the leak was fixed, so new measurements at the road to the east could be used.

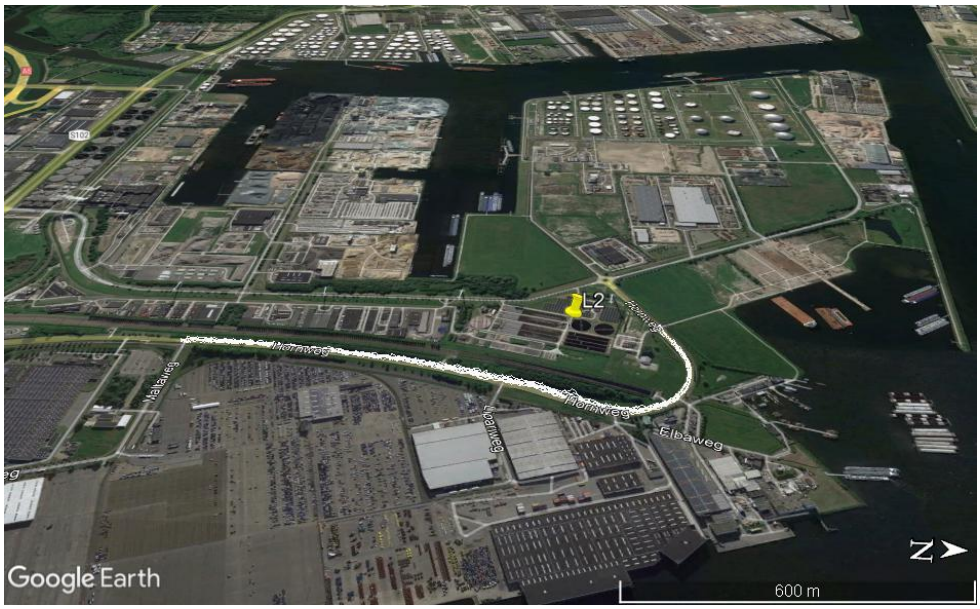

Figure 25. Wastewater Treatment Amsterdam Westpoort is a small WWTP serving the port area industry. Public roads surround it, but they are not all at perfect angles for transects.

8.1.4 Location 3: Wastewater Treatment Zaandam-Oost (WWTP)

The third WWTP is located north of the Noordzeekanaal, near Poelenburg, a neighbourhood in Zaandam. It has a capacity of 152.000 p.e., therefore being the smallest WWTP in the research area. It also belongs to another regional water authority, Hoogheemraadschap Hollands Noorderkwartier. The 2019 registered amount of methane emissions is 44.4 tons CH_4/y ((RIVM, 2022). Measurements were done on 28/02/22 on the N156, a busy road to the north of the WWTP.

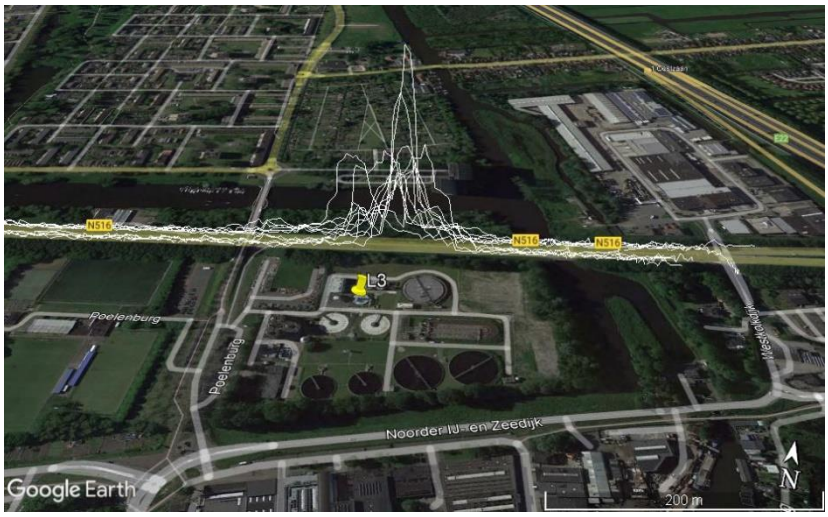

Figure 26. WWTP Zaandam. Compared to the other WWTs, this facility is in a more urban area, situated next to a bus station, a sports park, an industrial park and a residential neighbourhood.

8.1.5 Location 4: Bunge Netherlands (Food)

This location by Bunge Netherlands is a crushing and refining facility for plant-based oils, fats and proteins. The registered emissions for this facility are 6180 kg CH_4/y. It is possible to come close to the facility where emissions were detected. There were no suitable roads on a perpendicular angle to the facility, without any other significant facility in between. So there was no suitable wind direction for measuring transects.

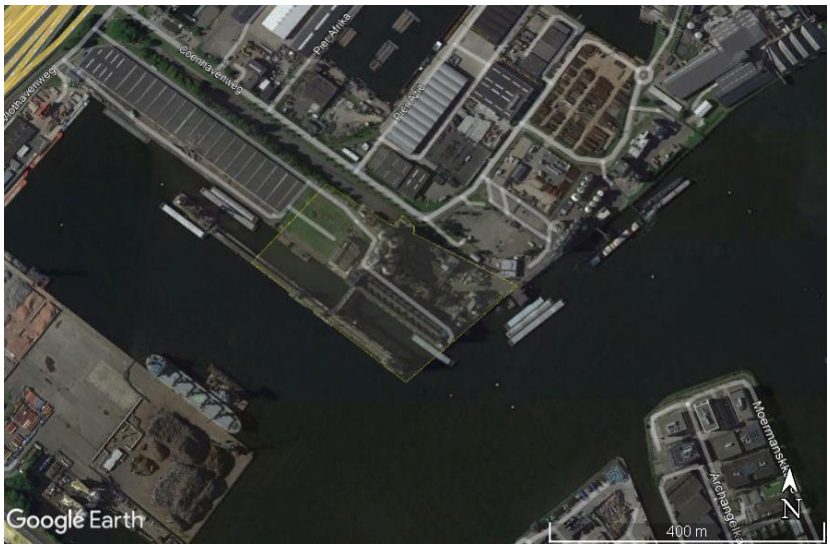

Figure 27. Bunge Netherlands. The facility is cornered between waterways and other industrial facilities. There is a public road ending at the facility, but no suitable roads around the facility for transects.

8.1.6 Location 5: Nuon Power Generation Hemweg (Energy)

This powerplant, operated by Nuon, is partially closed down with only a gas-fuelled component running. It is unclear whether the 2019 registered CH_4 emissions of 6180 kg/yr should still be expected. The facility is densely enclosed with streets, water and other facilities. There are multiple sets of building on the terrain with high chimneys. To the southeast runs the 12-lane highway A10, with tall windscreens and possible car combustion emissions. Therefore, transects across this highway are less reliable. A highway entrance/exit provided options to perform transects closer to the facility northeast of the highway. The S101/Nieuwe Hemweg, which runs southeast of the facility, and the Vlothavenweg, across the A10 highway, were also used for transects. Some CH_4 enhancements were observed during those transects, but they couldn't be attributed to the powerplant. More insight on the possible source location/height could help determine the best location to do measurements and verify the (lack of) CH_4 emissions.

Figure 28. Nuon Hemweg. This power plant has the large A10 highway situated to the south-east, and a smaller road S101 to the southwest. Transects did not indicate any clear emissions that could be attributed to this facility, but more research is needed for robust conclusions.

8.1.7 Location 6: Cargill (Food)

Cargill is a processor of raw food materials. It is on the waterside, with a small public road on the south. Measurements on this road showed some small CH_4 enhancements, but they were too irregular to be attributed or quantified. The facility has 2019 registered emissions of 3040 kg/yr.

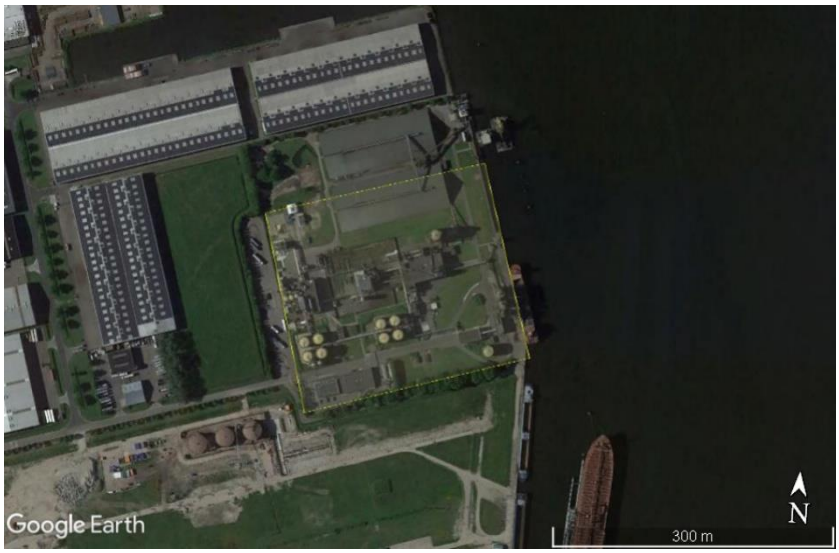

Figure 29. Cargill. This facility shows one small public road towards the water, SSW of the facility. Minor CH_4 enhancements were observed, but they were too small to do quantification.

8.1.8 Location 7: AEB (Waste)

Figure 30. AEB. This is a large waste furnace for the public waste service of the Amsterdam municipality. The location next to the largest WWTP and the curved road structure didn't allow any good transects. Methane enhancements were detected, but the exact source on the terrain could not be estimated.

8.1.9 Location 8: ICL Fertilizers Europe (Chemic. Ind.)

This transhipment and processing facility for fertiliser chemicals has 2019 registered emissions of 1300 kg/yr. The road structure did not allow good transects, as the facility is mainly surrounded by water. One public road leading to the facility entrance did enable the detection of CH_4 enhancements.

Figure 31. ICL Fertilizers. CH_4 enhancements were detected next to this facility, but there were no suitable roads for transects, as the facility is mainly surrounded by water.

8.1.10 Location 9: Sonneborn Refined Products (Chemic. Ind.)

Sonneborn Refined Products has 2019 registered CH_4 emissions of 1140 kg/yr. No methane enhancements were detected around this facility. A road to the south enabled transects, but the A5 highway was situated above this road (20-30 meters), which probably influences the plume dispersion too much for the GPDM.

8.1.11 Location 10: Main (Waste)

Main BV stores and transports fluid fossil fuels, has 2019 registered emissions of 590 kg/yr and is located on a small peninsula with dozens of tanks with fossil fuels. The roads on this peninsula were mostly private property, and it was unclear which of the tanks belonged to what company. There were no CH_4 enhancements detected around the peninsula.

Figure 32. Main BV. The tenth-largest emitter in the 2019 registered emissions. There are multiple companies with tanks of fossil fuels/chemical products, and it was unclear which tanks belonged to what company. Most of the roads on this peninsula were private property, and no methane enhancements were detected.

8.1.12 Location 11: Cabot Norit Nederland (Chemic. Ind.)

As this location was only 11th on the list of registered emissions, and the road structure did not allow any good transects with the most occurring wind directions, this facility was not visited for detection and quantification. The 2019 registered emissions were 130 kg/yr.

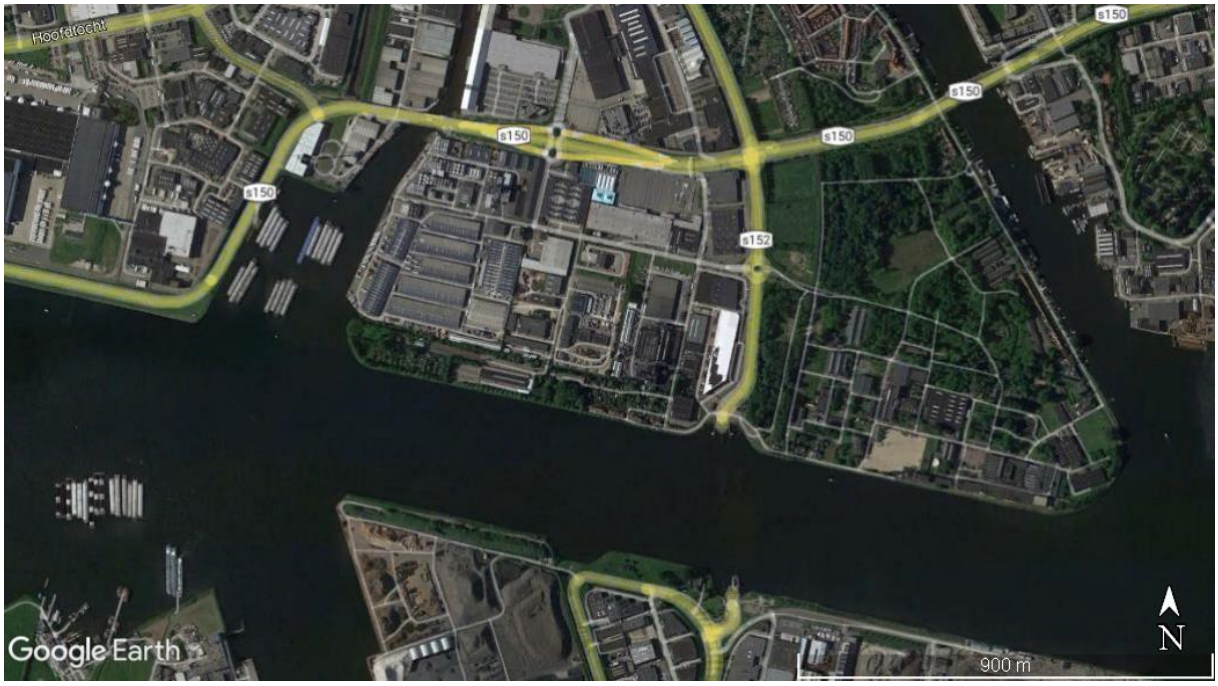

Figure 33. Cabot Norit. This facility was not visited for detection or quantification, as it was only possible with wind directions that occurred not often, and it had minimal registered emissions of 130 kg/yr.

8.1.13 Location 12: Oxea Nederland (Chemic. Ind.)

This facility was the last on the list with registered emissions, with a registered amount of 120 kg/yr in 2019. Most roads around the facility were private property. One of the roads that did come close is where the enhancements of Vosse Groen Recycling were detected. Other roads did not indicate any emissions coming from Oxea.

8.1.14 Location 13: OBA Terminal (Energy)

Figure 34 shows the OBA Terminal, a transhipment and storage location for coal, primarily transporting coal with trains to mainland Europe. The facility has a length of over 1300 meters, so measurements at a close distance often showed multiple peaks. There are two roads to the east of the facility. They are mainly parallel to each other, so the one at a larger distance is better for quantification. A road to the west, across a waterway and a storage parking or the transport of cars, was also used for transects on 02/03/2022 and 03/03/2022. Figure 34 shows that one transect on this furthest road gave significantly higher results. As the measured mixing ratio is higher than in most measurements on the closer roads, influence from other sources such as ships is probable.

As the width of the facility is smaller than the length, measurements at the north or south would improve the transects. Using a boat on the canal to the north might be a good option.

Figure 34. OBA Terminal. This coal transhipment facility extends far in the N-S direction. Therefore, the roads to the east often showed 2 peaks, indicating it is too close for the GDPM. The road to the west is at a larger distance, and the plumes on this road showed better gaussian shapes.

8.1.15 Location 14: Orgaworld (Energy/Waste)

Figure 35 shows Orgaworld, a producer of biogas, and the assumed point source location on this area of this facility. A small road only a few meters to the north showed strong methane enhancements, which attributed the emissions to this facility, but a road to the west was better for transects. Transects were measured on this road on 03/03/2022 and 15/03/2022. There were no registered methane emissions for this facility.

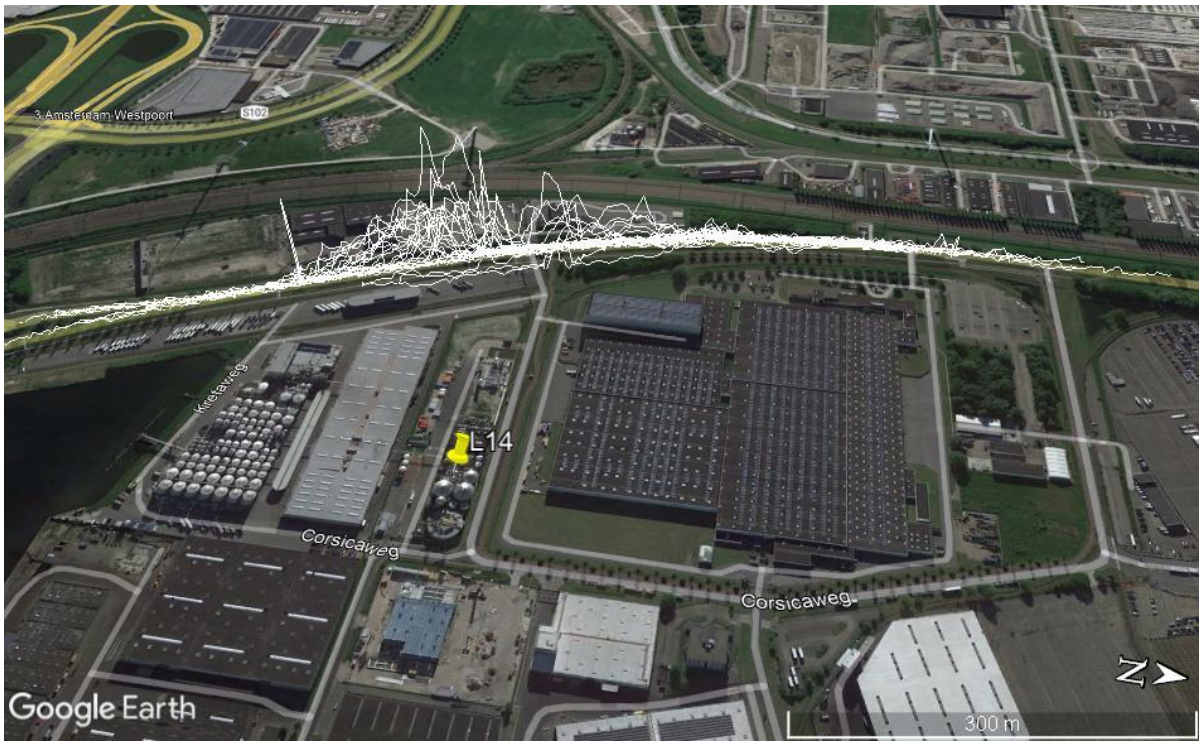

Figure 35. Orgaworld. The yellow pointer indicates the assumed point source on the Orgaworld facility. Only one road was used for transects to the west of the facility. Measurements on the north of the facility, only several meters from the source, attributed the emissions to this facility.

8.1.16 Location 15: Dutch Cacao (Food)

Figure 36 shows Dutch Cacao, a processing plant for cacao products with a chimney of 38 meters in height. The road directly next to the plant did not show any CH4 enhancements, whereas a road further to the west did show plumes more often, which confirms the plumes coming from a higher source. This facility had no methane emissions registered. But also on this further road, only 15 of the 39 transects showed enough transects to pass the quality check.

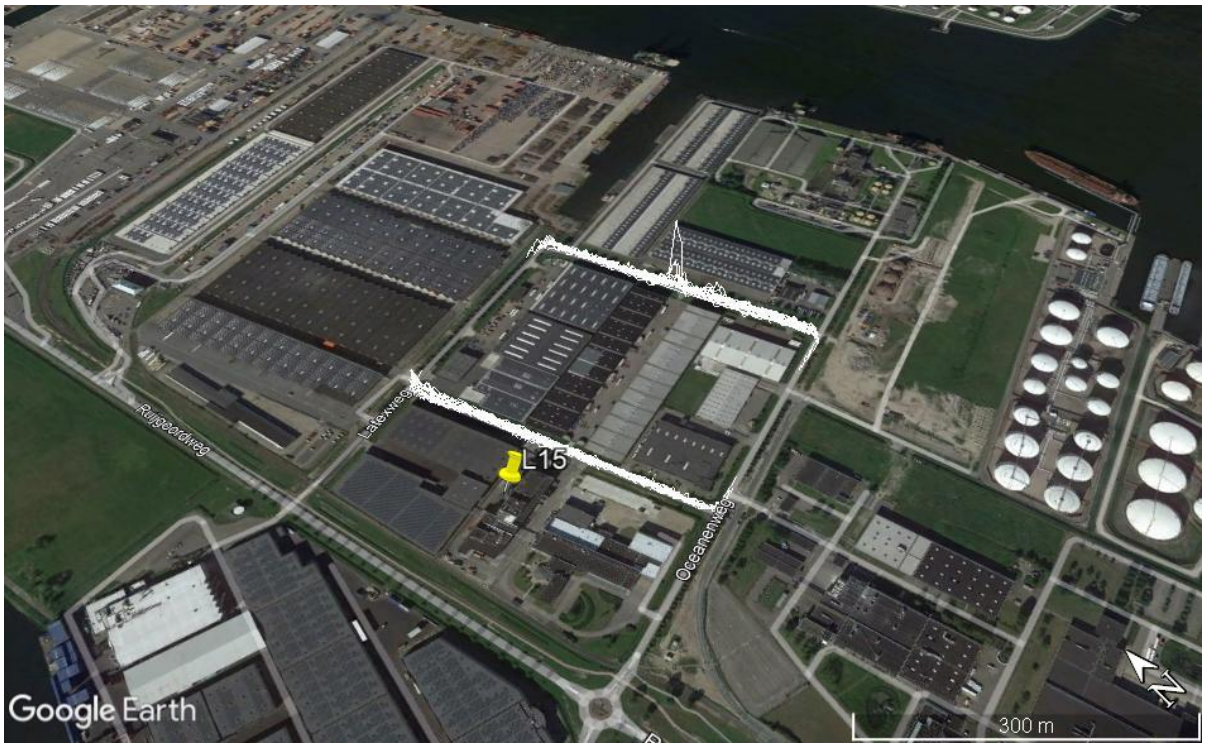

Figure 36. Dutch Cacao. The yellow pointer shows the location of the assumed source, a chimney with a height of 38 meters. The closest road never showed any measurements, whereas a road further to the east did show plumes more often.

8.1.17 Location 16: Paro Amsterdam (Waste)

Figure 37 shows Paro Amsterdam, a private collector and processor of waste with no registered emissions. This facility was not visited for transects, as there was no time with right wind directions. The road to the south is quite close to the source but might be good for transects when the wind comes from the north.

Figure 37. Paro Amsterdam. A private waste processor. No CH_4 enhancements were detected around this facility, but this location could be visited with northern wind for more robust conclusions

8.1.18 Location 17: Rietlanden Terminals (Energy)

Figure 38 shows the Rietlanden Terminals, with the transect measurements and the location of the assumed point source. This facility is the second coal transhipment location in the Port of Amsterdam.

Measurements on the S102, directly to the west, often showed multiple plumes. This improved when measuring on a small road further to the west, but this was just in front of a large hill (17 meters in height), which could lead to the accumulation of the plume. A further road across the water, to the west, had no other facilities in between and is thus the preferred location for measurements.

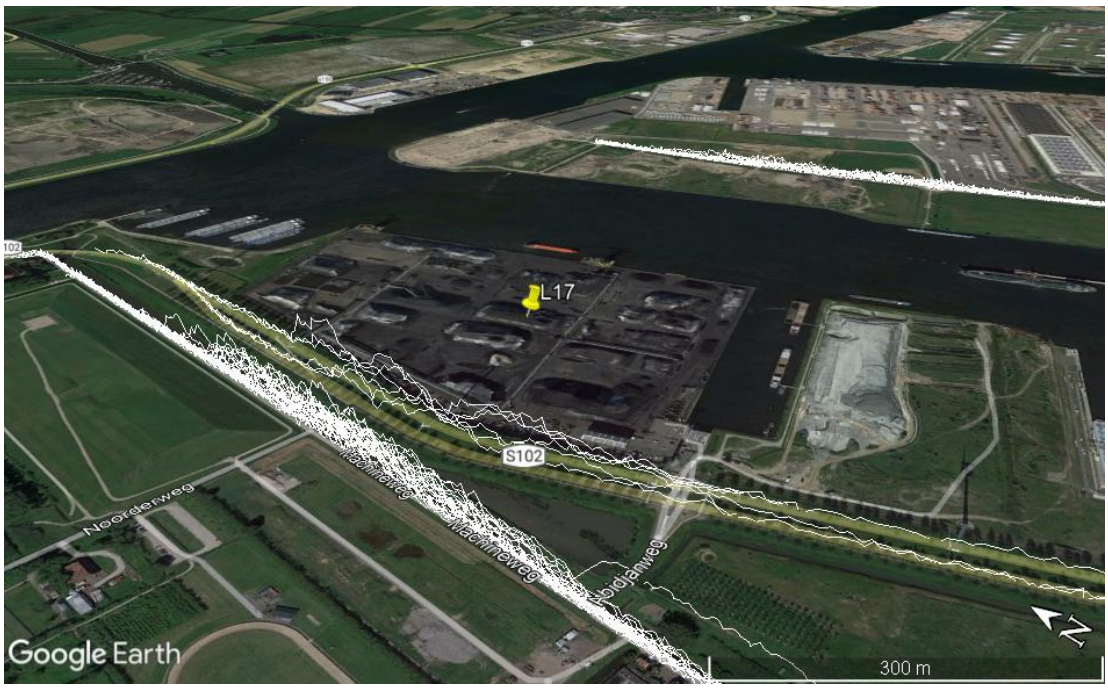

Figure 38. Rietlanden Terminals. The yellow pointer indicates the coordinates of the assumed point source in the middle of the facility. Measurements were done on a close road to the west, a parallel road somewhat further to the west, and a road across the water to the east.

8.1.19 Location 18: Vosse Groen Recycling (Waste)

Figure 39 shows Vosse Groen Recycling, a collector and processor of organic waste. The figure indicates the assumed point source location, which is only at 10 meters distance from the closest measurements. A second road is situated further to the east, which is more suitable for transects. This facility has no 2019 registered CH_4 emissions. The closest transects were measured on 09/02/2022, the furthest transects were measured on 17/03/2022.

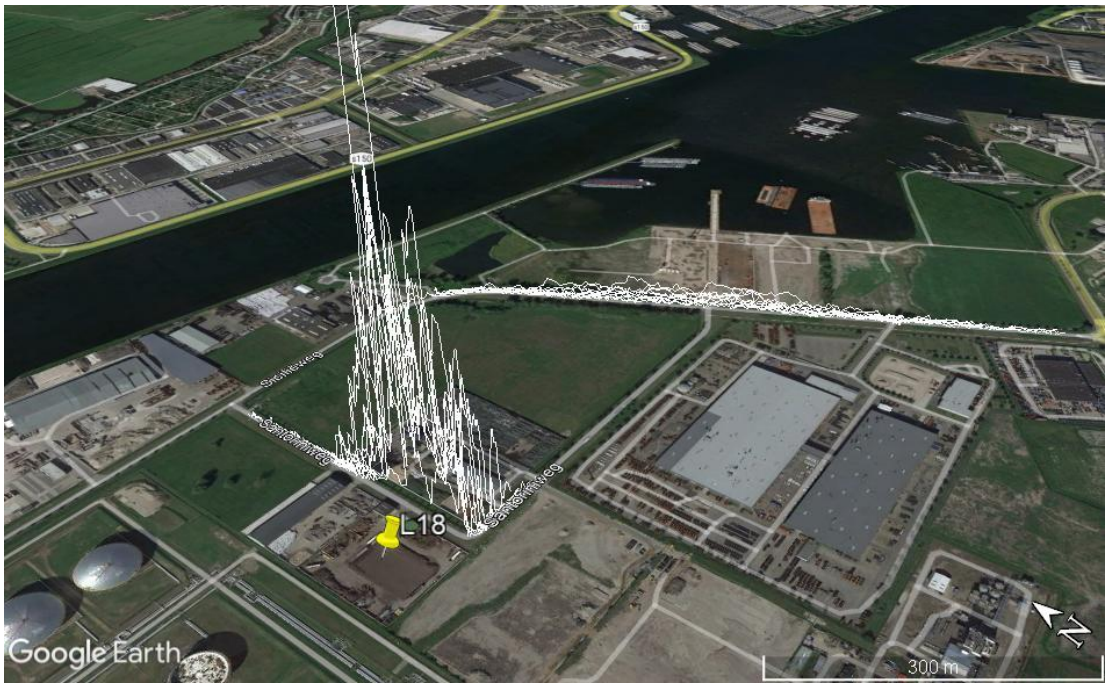

Figure 39. Vosse Groen Recycling. This facility processes organic waste materials. The assumed point source is indicated with the yellow pin, and the white lines show the measured CH_4 concentration of transects. The closest transects show larger concentrations

but are too close for good quantification. Therefore, the location further to the west is more suitable for transects, but this road was only used one day.

8.2 Appendix 2: Overview of measurement days

Table 7. An overview of all measurement days, together with some essential information. It shows the start and end times of the port area's visit and the Picarro instruments' delay times as measured at the beginning of the day. The meteorological data of Schiphol is shown to indicate the difference in meteorological conditions. It shows the average meteorological conditions during the transect measurements.

Dates	Start time (UTC)	End time (UTC)	Delay G2301 (s)	Delay G4301 (s)	Windspeed Schiphol (m/s)	SW Radiation Schiphol (W/m²)	Stability Class	Main wind direction
2021-12-02	09:30	12:30	68	-4	5.8	58	D	WNW
2022-02-07	09:30	13:30	-15	-4	8.0	322	D	WSW
2022-02-08	12:30	16:00	-16	-5,5	9.6	156	D	SW
2022-02-09	12:00	15:30	-15	-5,5	8.5	131	D	WNW-W
2022-02-10	12:00	16:00	-15	-8	6.5	82	D	NW
2022-02-11	12:50	15:00	-14	-8	5.0	258	D	SS
2022-02-28	09:45	13:30	-9	-2	6.4	486	D	ESE
2022-03-02	14:30	17:10	-7	-4	4.7	218	D	E
2022-03-03	13:00	15:30	-7	-4	5.0	417	D	ESE
2022-03-14	12:48	16:12	-46	-63	3.4	409	D	WSW
2022-03-15	12:15	14:45	-44	-63	3.0	544	C - D	ESE
2022-03-17	12:19	14:15	-40	-60	6.0	591	D	W
2022-03-29	12:20	14:30	-39	-3	4.0	537	C	NE
2022-05-13	09:00	13:00	-22	-72	8.8	734	D	W

8.3 Appendix 3: Supplementary method details

8.3.1 Picarro CRDS calibration

Picarro G2301:

$$CH_{4\,cal} = CH_4 * 1.0014 + 0.005 \quad (1)$$

$$CO_{2\,cal} = CO_2 * 1.0088 + 0.320 \quad (2)$$

Picarro G4302:

$$CH_{4\,cal} = CH_4 * 1.0043 + 0.033 \quad (3)$$

$$C_2H_{6\,cal} = C_2H_6 * 0.9950 \quad (4)$$

8.3.2 Quantification Flowchart

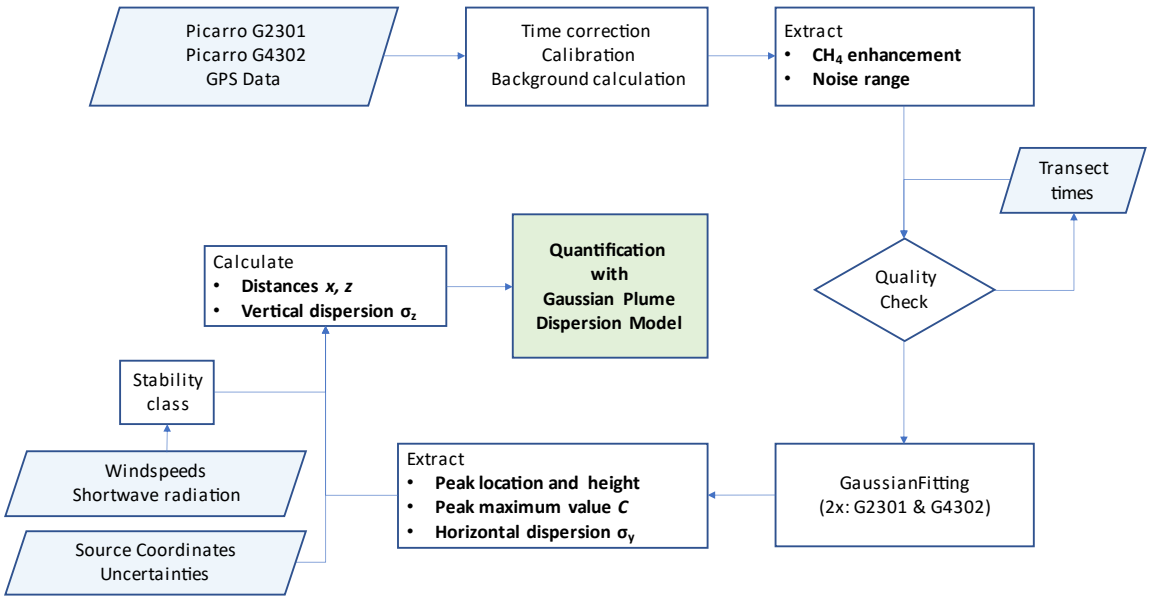

8.4 Appendix 4: Python script.

Two different files were used. The first script (Merge_Calibrate.py) was used to combine the different RAW data files and do the necessary corrections, calibration and background extraction. The second script (Trans_analysis.py) was used for all other data analysis and visualisation. Both files are added as supplementary files to this thesis. Contact Daan Stroeken if you want the files.